Wireless Dust Sensor Network for a Feedlot Dust Abatement Study

A THESIS
SUBMITTED TO THE FACULTY OF THE GRADUATE SCHOOL
OF THE UNIVERSITY OF MINNESOTA
BY

Scott Ryan Klar

IN PARTIAL FULFILLMENT OF THE REQUIREMENTS
FOR THE DEGREE OF
MASTER OF SCIENCE IN
ELECTRICAL AND COMPUTER ENGINEERING

SUPERVISED BY:
Dr. Taek Kwon

February 2016

Acknowledgments

Many thanks must be given to my advisor Dr. Taek Kwon for his support, patience, and encouragement throughout the duration of my Master's Degree.

I would also like to thank all of the faculty and staff at the University of Minnesota Duluth Department of Electrical and Computer Engineering for always being very accessible and for providing me with a good educational foundation.

Brent Auvermann and his research team at Texas A&M were very supportive during the research development. They provided the necessary details related to the research field of dust measurement and environmental conditions. They also were very supportive during my visit to Texas and facilitated my field testing.

And many thanks to Shey Peterson for guiding my enrollment processes, departmental paperwork, and moral support.

Abstract

The mobilization of animals across Concentrated Animal Feeding Operations (CAFOs) generates large dust plumes causing visibility and human health issues. Research studies currently use large, expensive sensor technologies to collect dust-air concentration measurements limiting data collection to just a few sampling points. The ability to measure with many sampling points across a field and to have vertical measurements would aid in the characterization of dust plumes by providing a more accurate, average concentration.

A small, inexpensive, portable, wireless nephelometer dust sensor was developed using a low-cost, commercial optical sensing module. A field study was performed using ten low-cost nephelometers at a cattle feedlot in Texas during a typical peak dust-air concentration. The initial error of the sensors was 7%, but gradually increased over time to 32% as dust accumulated on the optics. A second dust sensor was developed to improve upon some of the limitations of the nephelometer sensor. This sensor samples air by the method of impaction of a dust-air stream into a water droplet and dust images are captured using a low-cost USB microscope. A software algorithm was developed that differentiates dust from the image background finding the mass and diameter of the dust particles. Lab testing indicated that data from this sensor trends well against reference sensors.

The Box Model was used to calculate the emissions from measured concentrations at a source location and a Gaussian Dispersion Model predicted the concentration at a downwind location. Using air dispersion modeling, having at least six portable sensors with up to 20% measurement error in a 100 meter square field can result in increased accuracy over a single point measurement in calculating the average dust plume concentration.

Table of Contents

List of Figures vi
List of Tables viii
Chapter 1: Introduction 1
1.1 Motivation 1
1.2 Objective 3
1.3 Review of Current Technology 3
1.3.1 TEOM 4
1.3.2 Gravimetric Sample Collection 5
1.3.3 Laser Diffraction 7
1.3.4 Light Scattering 7
1.4 Related work 8
Chapter 2: Wireless Nephelometer Network 11
2.1 Nephelometer Sensor Design 11
2.2 Network Topology 14
Chapter 3: Microscopic Dust Sensor 17
3.1 Microscope Sensor Overview 17
3.2 Microscope Sensor Construction 18
3.3 Software Design 20
3.4 Image Processing Algorithm 21
3.5 Connected Component Labeling 23
3.6 Particle Sizing 25
Chapter 4: Dust Chamber Design for Sensor Testing 27
4.1 Hardware Introduction 27
4.2 Dust generation chamber 27
4.2.1 DGS Operation 28
4.2.2 Construction Detail 30
Chapter 5: Experimental Results 33
5.1 Calibration Procedure for Nephelometer 33
5.2 Nephelometer Field Test 36
5.3 Microscope Sensor Lab Test 39
Chapter 6: Air Dispersion Modeling for Evaluation 43
6.1 Box Model 44
6.2 Gaussian Model 45

6.2.1 The Effects of the Ground on the Gaussian Model 47
6.2.1 Effect of Air Dispersion Coefficients 48
6.3 Modeling Dust Plume with Box and Gaussian Models 49
6.3.1 Uniform Distribution 50
6.3.2 Normal Distribution with Single Sensor 51
6.3.3 Normal Distribution with Sensor Network 52
Chapter 7: Conclusion 59
7.1 Future Recommendations 60
References 62
Appendix A Nephelometer Hardware Specification and BOM 66
Appendix B Microscope Sensor BOM 69
Appendix C DGS Bill of Materials 70

List of Figures

Figure 1: Dust inhalation effects, (source ref [13]) 1
Figure 2: TEOM sensor operation, (source ref [6]) 5
Figure 3: Impactor particle sizing 6
Figure 4: Light-scattering instrument 8
Figure 5: Wireless sensor and datalogger circuit boards 12
Figure 6: Packaging the nephelometer sensor 12
Figure 7: Nephelometer and battery stacked 13
Figure 8: Ten nephelometer sensors assembled for field testing 14
Figure 9: Star wireless network 14
Figure 10: Extending wireless network with a router node 15
Figure 11: Wireless mesh network topology 16
Figure 12: Impaction principle 17
Figure 13: Custom microscope slide 17
Figure 14: Microscope sensor components 18
Figure 15: Microscope sensor prototype 19
Figure 16: Image collection software 20
Figure 17: Sensor control logic 21
Figure 18: Background subtraction and threshold test image 22
Figure 19: Image pixel value histogram 22
Figure 20: Connected Component Labeling search pattern 24
Figure 21: Initial testing of the CCL algorithm on simulated data 25
Figure 22: Dust generation and sampling system 28
Figure 23: Dust generation system diagram 29
Figure 24: Intake components 30
Figure 25: Settling/sampling chamber components 31
Figure 26: Exhaust components 32
Figure 27: Nephelometer data pre-calibration 34
Figure 28: Isolating tail portion of nephelometer data 35
Figure 29: Performing linear regression of nephelometer data 35
Figure 30: Nephelometer calibration results 36
Figure 31: Nephelometer field test at a Texas feedlot 37
Figure 32: Nephelometer field test data 38
Figure 33: Nephelometer residual effect 38
Figure 34: Image pixel value histogram 40
Figure 35: Microscope sensor and DustTrak measurements 41
Figure 36: Microscope sensor accumulated mass 42
Figure 37: Air pollution model basic parameters 43
Figure 38: The Box Model parameters 44
Figure 39: Coordinate system and representation of Gaussian Model 46
Figure 40: Effect of air dispersion coefficients 48
Figure 41: Uniform distribution source concentration 50
Figure 42: Gaussian downwind concentration from uniform source distribution 51
Figure 43: Normally distributed source concentration 51
Figure 44: Single sensor error vs. sensor position 52

Figure 45: Box Model sensor placement 54
Figure 46: Estimating plume with six network sensors 54
Figure 47: Scaling six sensor trendline for reference sensor 56
Figure 48: Box Model with time-varying plume 57
Figure 49: Modeling time-varying plume 58

List of Tables

Table 1: Microscope Sensor Specifications……...20
Table 2: CCL Equivalency Table 24
Table 3: Nephelometer Standard Deviation..... 39
Table 4: RMSE Calculation for Nephelometer and TEOM Data 39
Table 5: Dispersion Coefficients..... 48
Table 6: Network Sensors Plume Accuracy 55
Table 7: Network Sensors and Reference Sensor Plume Accuracy..... 56
Table 8: Network Sensors Time-Varying Plume Accuracy 58

Chapter 1: Introduction

1.1 Motivation

Concentrated animal feeding operations (CAFOs) have been a proven method of raising cattle to supply the beef industry. They have been growing the number of head per pen and total feedlot size; in fact the Cattle Empire LLC in Southwest Kansas has a total one-time capacity of 229,000 head of cattle in five feedyards [1]. Dust emissions from feedyards is a growing concern among ranchers, neighbors, and regulatory agencies such as the Environmental Protection Agency (EPA). The Clean Air Act, last amended in 1990, requires the EPA to set National Ambient Air Quality Standards (NAAQS) standards for pollutants considered harmful to public health [2]. Particle pollution is among one of the six pollutants listed. Pollution levels are set for PM2.5 and PM10 (particles smaller than 10 micrometers in diameter) particles.

Airborne emissions classified as PM10 dust particles are considered harmful because particles smaller than 10 microns have the ability to travel deep into human lungs. Three classifications of dust depicted in Figure 1 are: inhalable, thoracic, and respirable [3]. Inhalable is the fraction of dust that can enter the nose and mouth measures up to 100um in diameter. Thoracic is the sub-fraction of inhalable dust that that penetrates into the respiratory tract below the larynx up to 10um diameter. Respirable dust is less than 4um in diameter and can enter the aveolar regions of the lungs.

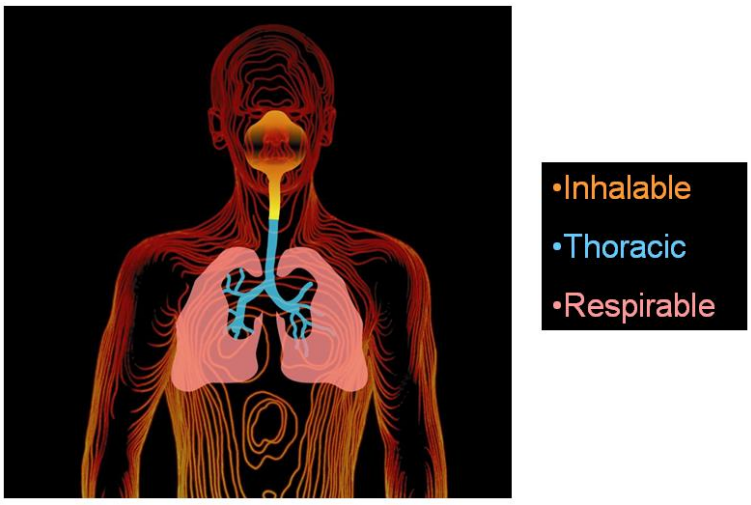

Figure 1: Dust inhalation effects, (source ref [13])

Dust emissions may consist of gases like ammonia, hydrogen sulfide, or volatile organic compounds as well as particulate matter consisting of microbial organisms or biological aerosols, dried manure, mold spores, bacteria and viruses. Direct health effects as a result of exposure to high concentrations of PM10 dust are currently an area of study that has much to be discovered. It is known to commonly enhance allergies and trigger asthma attacks.

Even without the full understanding of all health effects related to dust, the World Health Organization defines health as a state of complete physical, mental, and social well-being, and not merely the absence of disease or infirmity [4]. Therefore, it is up to regulators to maintain standards that allow ranchers, agricultural workers, and neighborhoods to coexist without ill effect.

Feedyard studies help collect the science related to dust generation and control. Science allows for informed decisions to be made. Setback estimation tools, developed using data from these studies, exist to help policy makers analyze the possible impact to neighbors and public areas when a feeding operation owner thinks about expanding their operations [5]. The estimation tools can suggest various methods to combat spread of pollution: Lagoon covers, wind breaks, filters, diet and feed management.

In 2008 the US EPA published a final ruling that forces certain livestock facilities to report their air emissions. Setting limits on airborne emissions and researching health effects require that PM10 dust be measured. There are many sensors available on the market to measure dust. One thing they all have in common is that they are very costly. Therefore, the type of data to be collected must be carefully selected to determine the appropriate sensors.

A common data type shown by many researchers is 24hr average emission concentrations along with the time-varying concentration – the relative measure of daily concentration patterns showing the evening dust peaks and meteorological data. Measuring height and shape of the dust plume is a desired output as well. Meteorological conditions used to calculate mass-air concentrations are: wind speed, direction, ambient temp, stability class, mixing height.

1.2 Objective

One objective of this thesis is to provide a research team from Texas A&M University with a low-cost dust sensor network that shows time-varying dust-air concentrations. The sensor should allow the team to more easily and less expensively characterize the daily dust plume surrounding a cattle feedlot. To accomplish this they must be small and portable to allow for placement at various locations across a feedyard that is perhaps several hundred meters wide. The sensors may be placed vertically as well to measure the dust plume concentration at several heights.

Small, low-cost, portable sensors that can be wirelessly networked across a field have some unique advantages even if the sensor resolution is lower than sensors recommended by regulatory agencies. The wireless ability of the sensor to form an expanding network allows researchers to place them in any pattern over a large area to target the measurement points of interest. The small size of the sensors promotes placing them vertically on a pole, structure, or even to be elevated by a balloon. Previously studies have collected concentration data of dust plumes by flying a small airplane in a zig-zag pattern over the plume and immediate downwind area. The ability to more easily measure plume height would give valuable data toward setting the height used in the Box Model calculation for emission flux from the ground-level source.

1.3 Review of Current Technology

To classify a dust plume around a feedyard many sensors are needed to determine the width and height of the plume. The size and cost of many sensors prohibit the measurement of these aspects, for example, an Environmental Protection Agency (EPA) accepted sensor called the Tapered Element Oscillating Microbalance (TEOM) measures PM10 dust, but is very large, heavy, and expensive starting at around $10,000. They require a high voltage power source, and protection from physical damage such as cattle rubbing against the enclosures. Protective cabinets are installed around the sensor and it must be air-conditioned to maintain accurate readings. Commonly used sensor technologies are the TEOM, gravimetric filter analysis, laser diffraction, and light scattering,

1.3.1 TEOM

One of the generally accepted sensor technologies approved by the EPA is the Tapered Element Oscillating Microbalance (TEOM) shown in Figure 2, which measures PM10 concentrations in real-time. It consists three main parts: The sample inlet head allowing PM10 size dust pass into the instrument, the TEOM sensor containing the microbalance and filter, and a controller to monitor and record the mass and air flow data as well as other measurements like temperature and barometric pressure [6]. A spring-mass equation, shown in Eq. (1), is used to model the particulate mass.

$$F = \sqrt{(K_0}/M) \tag{1}$$

Where,

F = frequency of oscillation (Hz)

K_0 = spring rate (N/m)

M = total mass of the tapered element, filter cartridge and particulate (kg)

Actually, the TEOM determines change in mass. The TEOM measures the oscillating frequency of a hollow tapered element to determine the dust mass collecting on a filter. K_0 is determined by the sensor manufacturer by installing two separately weighed filters and measuring the change in frequency. Equation (1) can be rearranged to solve for change in mass as shown here in Eq. (2).

$$\Delta M = K_0 \left(\frac{1}{{F_1}^2} + \frac{1}{{F_2}^2} \right) \tag{2}$$

Where,

ΔM = change in mass (kg)

F_1, F_2 = initial and final measured oscillation frequencies (Hz)

Data is recorded as Total Particulate Mass (TPM) accumulated on the filter every 2 seconds and Total System Mass (TSM) at the end of each 2-second period, plus the initial mass of the system at the time sampling began. This data is usually smoothed to 5-minute intervals before being recorded.

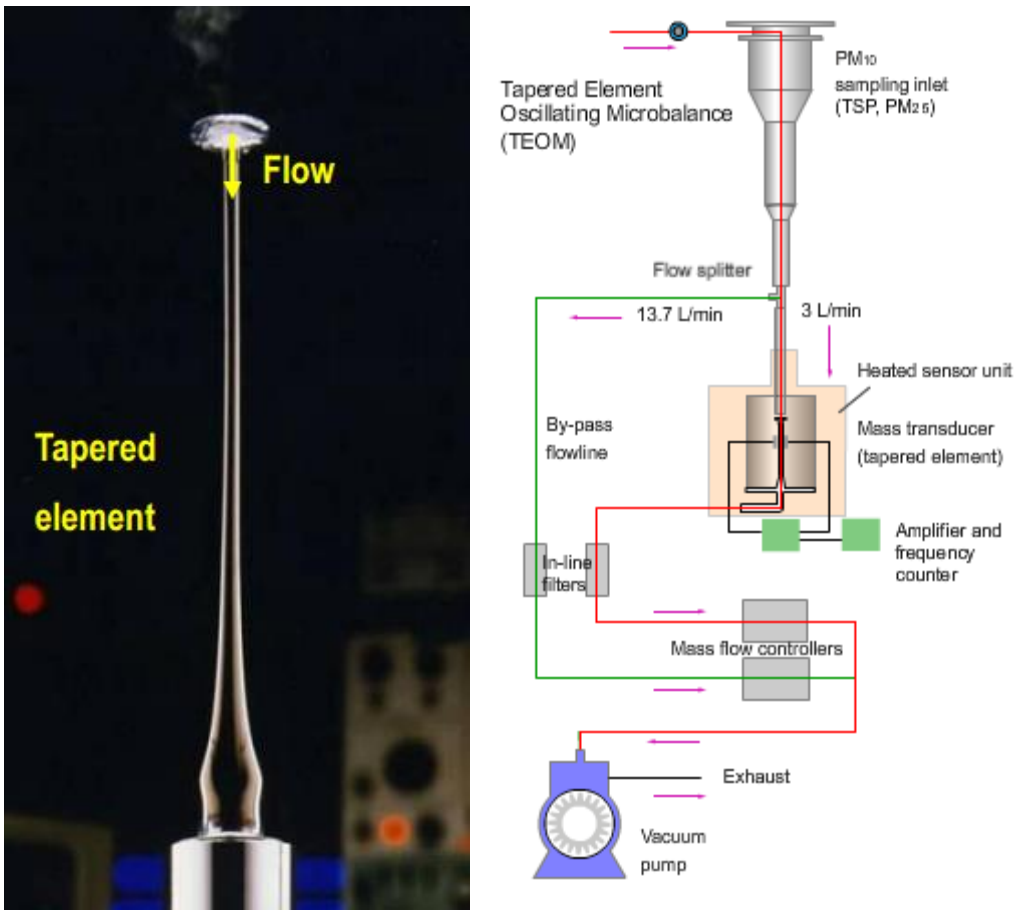

Figure 2: TEOM sensor operation, (source ref [6])

1.3.2 Gravimetric Sample Collection

Gravimetric sampling involves moving a fixed flowrate of air through a collection filter. Two types of dust filters are pre-weighed and matched weight and usually made of polyvinyl chloride (PVC) [7]. Pre-weighed filters are weighed at a consistent temperature and humidity also called equilibrated. After the sampling period the filters are again equilibrated and the post sample weight is determined. The difference between the initial weight and the final weight and the volume of air sampled is reported in mg/m^3. Matched weight filters do not require initial weighing. Two filters of equal weight are placed one on top of another during sampling. Dust collects only on the top filter so the number reported is the difference between the weights of the two.

To isolate the sampled dust to a certain size, impactors or a Dorr-Oliver cyclone

can be attached to the inlet of the instrument. An impactor, shown in Figure 3, separates dust from the air sample by forcing the air around a tight bend. Particles too large have too much momentum to flow around the bend, and impact a plate intended to hold these particles. Smaller particles follow the airstream to the sensor area.

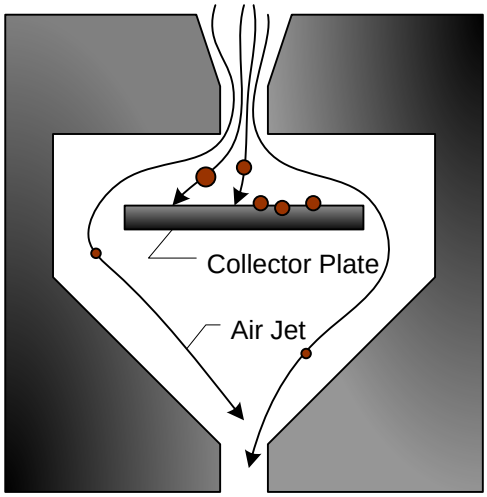

Figure 3: Impactor particle sizing

A Dorr-Oliver cyclone is designed to separate respirable dust from non-respirable dust; passing a range of 0.2-10um size particles. A cyclone works to separate dust from air by forcing air in through an inlet port in a direction that rotates the air. Centrifugal forces push the large particle outward to the cyclone wall and then they fall down to a collection chamber. Smaller particles are able to fill the center of the rotating air column and move up and out of the chamber through an exit port in the center of the cyclone. The air flow rate and the geometry of the cyclone determine the cutpoint. Cutpoint means the size of the particles that will be removed with a 50 percent efficiency.

OSHA has procedures for collecting and calculating the daily time-weighted average (TWA) dust exposure specifically for cotton dust [8]. They recommend 6-hour collection to represent the exposure a worker might see during a shift. A recommended instrument for collecting TWA dust exposure is a Lumsden-Lynch vertical elutriator. A flow rate of 7.4 liters per minute is specified through a 5 um, 37mm diameter polyvinyl chloride (PVC) membrane filter. A balance sensitive to 10 micrograms should be used for mass measurement.

1.3.3 Laser Diffraction

Another widely used real-time particle measurement technique is called laser diffraction. Some of the main reasons for its success are: wide measurement range from submicron to millimeter range, fast measurement results in less than a minute, repeatability from a large number of particles are sampled in each measurement, and calibration is not necessary [9]. The Mastersizer series is a popular particle size analyzer made by Malvern Instruments. This instrument requires 120V power at 50 watts, so it is not intended for field use and would require special power installation to each unit. They are smaller than the TEOMs at about the size of a piece of luggage. The basic Mastersizer 3000E starts at $40,000 limiting the total number of sensors afforded in a typically funded research project.

Laser diffraction uses angular variation of intensity of light to measure particles. A laser beam passes through a dispersed stream of particulate; large particles scatter light at small angles and small particles scatter light at large angles onto a series of detectors. This is based on the MIE theory of light scattering. The particle size distribution is reported assuming a volume equivalent sphere model. MIE theory requires knowledge of the optical properties of the particle under measure. This is usually found from published data or from built-in databases included with modern measurement equipment. If the optical properties are not known they can be estimated using an iterative approach based upon goodness of fit between collected data and data from other measurement devices.

1.3.4 Light Scattering

The TSI DustTrak™ is a basic photometric instrument used to determine the mass concentration of aerosols in real time [10]. A diaphragm pump, shown in Figure 4, moves a continuous stream of air into the sensing chamber. Part of the aerosol stream is split and sent through a HEPA filter. This cleaned air passes around the inlet nozzle as a sheath flow to help keep the optics clean. The remaining aerosol passes through the inlet into the sensing chamber where it is illuminated by a sheet laser light. A spherical mirror captures a large portion of the light scattered off particles and focuses it onto a photo detector. The photo diode outputs a voltage proportional to the mass concentration of the aerosol. The voltage is multiplied by a calibration constant which is usually determined with a known

particulate sample.

Calibration can be further improved by gravimetric sampling running alongside the photometric samples. Some DustTrak models allow a filter cassette to install in line with the aerosol stream to perform gravimetric analysis. Impactors can also be installed on the air inlet to separate dust into various size categories: 1, 2.5, 4, and 10 microns or less in size.

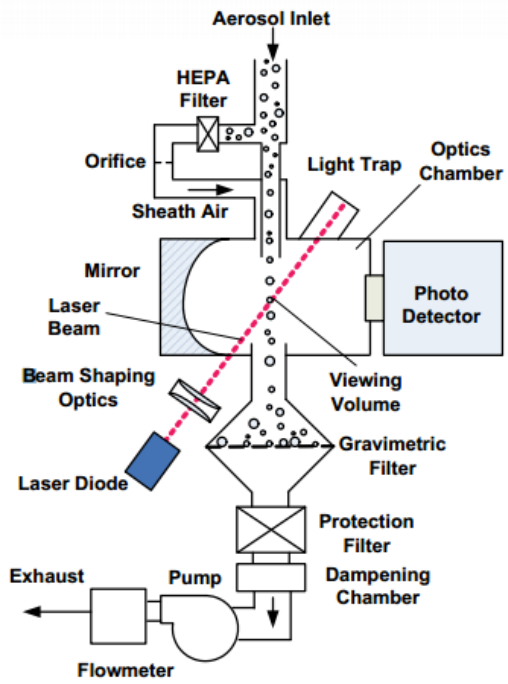

Figure 4: Light-scattering instrument

1.4 Related work

A majority of studies related to the design and testing of low cost dust sensors cite issues related to human health as their motivation. Health issues sensitive to dust are Pulmonary Disease Management, Asthma, and Chronic Obstructive Pulmonary Disease (COPD). Attacks can be triggered by certain dust, temperature, and humidity variations. Personal environment monitoring could support notifying the patient in advance of possible attacks [11].

Some sensors were designed as wearables for portable personal monitoring. An example is a sensor worn on the waistband of a person. It wirelessly connects to a phone or PDA to provide a user interface and data storage [11,12].

People occupy both indoor and outdoor environments. It appears that very limited work has been performed in an outdoor environment. The reason is likely that outdoors is more challenging due to weather elements like wind, rain, hot and cold temperatures, and UV from the sun, as well as small insects and larger animals contacting the sensor. Mainly testing has been performed indoors where the environment is more controlled and it is easier to study the correlation of the sensor results to reference sensors.

A common theme for dust sensor studies is to have a network of low-cost sensors to accurately model the environment. A single point source of measurement does not describe the air quality with certainty. Many measurement points and even redundancy increase the certainty of the data. To form a network of a dozen or more nodes the sensor design must be inexpensive. Light scattering methods using off-the-shelf sensors interfaced with simple control circuits were attempted in various research. Budget optical sensors commercially available and used in related studies were: Shinyei PPD42NS and PPD-20V, Sharp GP2Y1010, Samyoung S&C DSM501A. One study used a First Alert SA302 sensor from a smoke detector that combines ionization and optical detection [13]. Another study proposed using the principle of vibration with theoretical calculation supporting this idea [14]**.** Affordable reference sensors used in these studies were: Dylos DC1700, Met One Instruments Bam 1020, GRIMM OPC Model 1.108, TSI DustTrak II model 8530, and DustTrak DRX 8533.

One study focused on building a mobile multi-sensor platform called the TECO Envboard intended to be used as a research and development platform to aide in investigating different research questions like the suitability of commodity dust sensors for particulate matter measurement [15]. The array of sensors includes: particulate matter (PM10), carbon dioxide (CO_2), oxygen (O_2), volatile organic compounds (VOC), methane and chlorofluorocarbons (CFC), atmospheric pressure, acceleration, noise, ambient light, temperature, humidity, GPS location, and more.

An indoor test was performed with the TECO sensor in a research facility near a doorway. A DustTrak DRX 8533 Aerosol Monitor from TSI was used as a reference. The first ten minutes of the test was used to calibrate the sensors to the reference using a linear calibration offset. A 12-hour sampling session then followed. A comparison of data was performed using Mean Absolute Error (MAE). Averaging the sensor data to five-

minute periods allowed the MAE to be within 20 micrograms per cubic meter. They concluded that at least a coarse estimation of particulate matter can be determined using these low-cost sensors.

Another study was conducted in a heavily travelled corridor on the Berkely campus [16]**.** Cameras were mounted at the sensor sites to keep track of when people passed by the sensors so they could trend the dust data with human activity. The sensors were calibrated to an Optical Particle Counter (OPC) over a 29-hour experiment. They found an MSE of 9.5% for particles with diameter over 2.5 micrometers. A suggested alternative use for the dust sensor is as an occupancy detector in place of passive infrared sensors.

Other sensor designs are built intending to be more like consumer items. The PiMi Air Box is a standardized design for the team of Electrical Engineers from Beijing, China that has shipped to volunteer users across China and has logged over 50,000 hours of indoor dust concentration data [17]. It is calibrated in a controlled environment with PM2.5 dust to professional equipment.

InAir is another sensor design involved in participatory studies [18]. The sensor was linked to an IPad tablet for visual display to the user. It was concluded that when people see immediate effects of the dust-air concentration based on their activities, that they might change their behavior slightly in efforts to reduce the dust concentration readings on the IPad display.

The M-DUST is a hardware module that can detect smoke, pollen, and dust concentration above 0.5 ug/m3. It has a vacuum pump to control the flow rate and attachable filters [19].

The PANDA (Portable and Affordable Nephelometric Data Acquisition) system had an R^2=0.72 using a least squares regression to a reference sensor on a 24-hour study [20]. They stated that when there are differences in measurements it is unclear whether there were actual differences in measurements at each point of measurement or if there were differences in particle size distribution or optical properties.

Chapter 2: Wireless Nephelometer Network

2.1 Nephelometer Sensor Design

The purpose of this project was to develop a small, low-cost, wireless, and battery powered dust sensor. These sensors should be easily deployable as a distributed network of sensors for measurement of vertical and horizontal distribution of fugitive dust. A low-cost OEM model GP2Y1010AU0F from SHARP Corporation was used as the basic sensing element for light-scattering measurement and a Digi XBee wireless module was integrated for wireless communication. The performance specification of the developed nephelometer sensor and component BOM is shown in Appendix A.

Two custom circuit boards are shown in Fig. 5. A sensor board uses a microcontroller to interface some analog circuitry with the Sharp sensor, an XBee wireless module, and a small fan. The total power consumption is less than 0.5W. The second circuit board is a data logger containing a wireless receiver, a real-time clock, an SD memory module, and connection to a PC. The data logger can operate in lab mode or field mode. Lab mode collects the data and connects it to software in a PC for storage. A real time graph of the sensor data is displayed on a computer monitor to give the operator instant feedback. For field implementation, a 2GB SD memory module is used as the data logger eliminating the PC. The data is stored as comma-separated values in files that can easily be opened in a spreadsheet program.

The wireless radio attached to each sensor allows placement anywhere inside a dust chamber without concern with wires and drill holes through the walls of the settling chamber. Also, the wireless monitoring increases safety by allowing the operator to be away from direct exposure to the dust plume in field applications. The XBee protocol can form an extended range network if configured with mesh network routing. This allows the user to gather sensor data from a variety of spatial configuration covering a large area. Figure 5 shows features of the circuit boards.

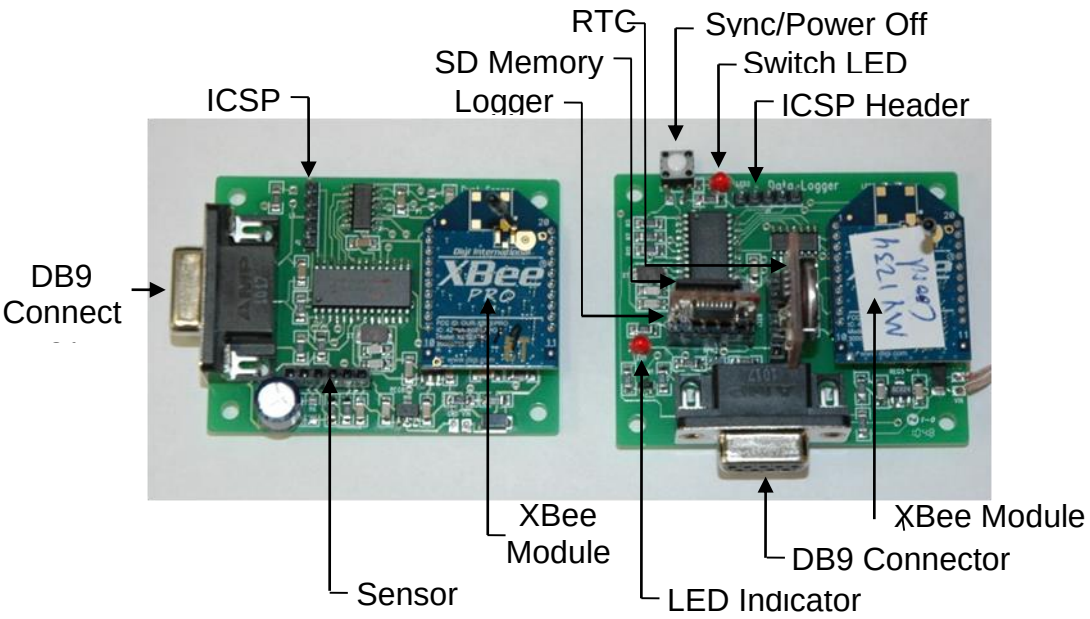

Figure 5: Wireless sensor and datalogger circuit boards

The Sharp sensor and circuit boards were placed into a compact and durable package shown in Fig. 6 to facilitate placement in field application where environmental conditions are a challenge to typical lab equipment.

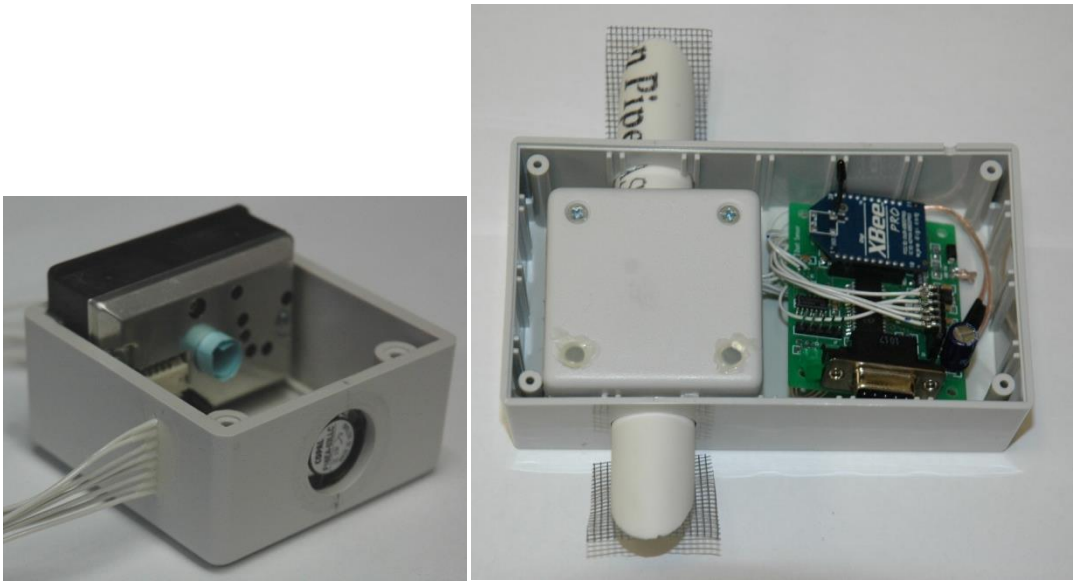

Figure 6: Packaging the nephelometer sensor

The optical sensor and fan were fastened to a small plastic box to create the sensing module. This is placed into a larger plastic box along with the circuit board. Intake and exhaust ports were angle cut and screened to prevent water droplets and insects from entering the sensing area. A battery was housed in a similar box so the units could be stacked as in Fig. 7.

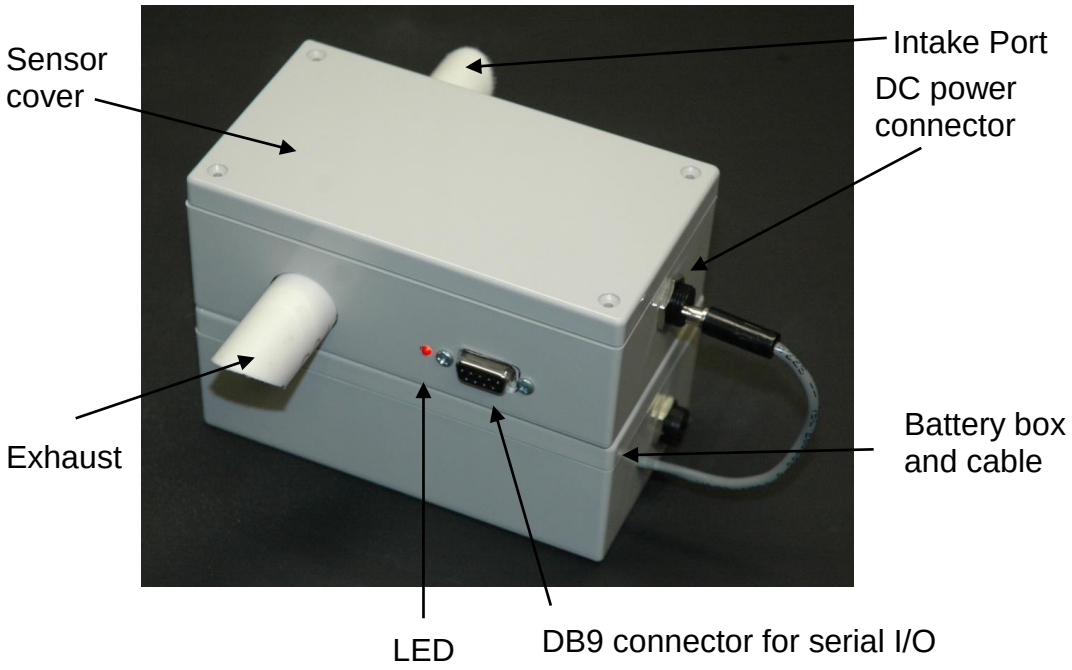

Figure 7: Nephelometer and battery stacked

Ten sensors and ten battery packs were built for field testing (Fig. 8). For extended test periods, one battery can plug into the next placing them in a parallel circuit. This will double the sensor operating time.

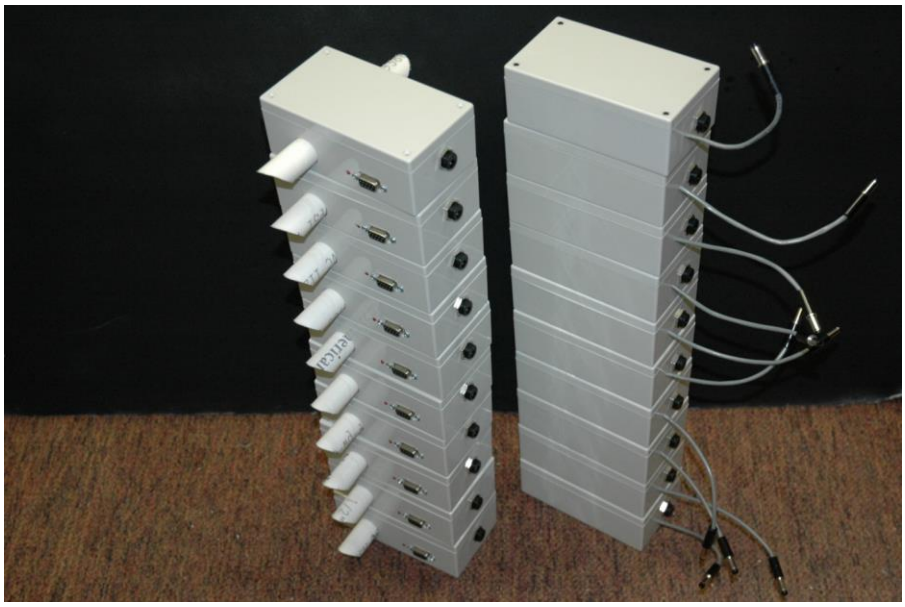

Figure 8: Ten nephelometer sensors assembled for field testing

2.2 Network Topology

The sensor network consists of multiple dust sensors and one data logger. The data logger acts as the central hub of a star network configuration (Fig. 9). The sensors act as end devices, and are physically placed anywhere around the data logger within wireless range. Each sensor is allowed to sleep between data transmissions to reduce power consumption. The sensor wakes the XBee module when it is ready to send a data packet. The data is transmitted to the data logger, and the sensor returns to low-power sampling mode.

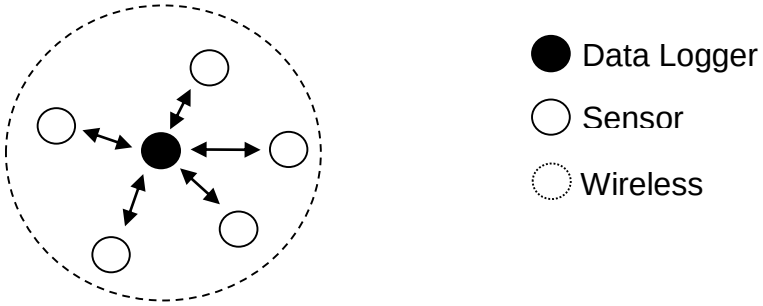

Figure 9: Star wireless network

Future work may be performed to extend the range of the network. Routers can be placed near the edge of the wireless range to create a larger range as shown in Fig. 10.

This forms a cluster, or tree network. Each node still maintains a single communication path to the data logger, but can use other nodes to route the data to the data logger.

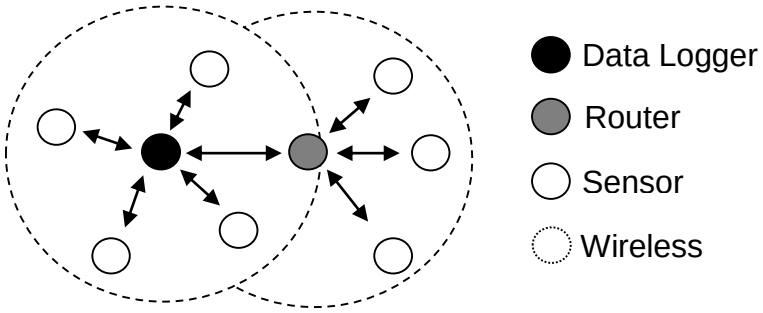

Figure 10: Extending wireless network with a router node

Wireless Mesh Sensor Networks (WMSN) are a network type that works well for creating networks with initially unknown size is a mesh network. WMSN's can forward packets of data using the optimal path without the concern of time slots and reducing the latency. An almost unlimited number of nodes are allowed (2^{64}) and there can be 100 meters between each node.

ZigBee is a mesh network protocol intended for applications with low-cost, low power consumption and low data rates. It is often used on sensor applications for the aforementioned reasons. ZigBee defines the application and security layer specifications enabling interoperability between products from different manufacturers using the wireless standard IEEE 802.15.4. There are over 150 companies using ZigBee and is actively promoted by several companies: Ember, Freescale, Honeywell, Mitsubishi Electric, Motorola, Philips, Samsung, and Texas Instruments.

Sensor networks can form several network topologies including star, tree, ring, and mesh. A mesh network is defined by the ability for each node to communicate with every other node in the network. Each node establishes a link to another node. When a network has hundreds of nodes and maintaining all those links becomes too burdensome, the network can be reconfigured with coordinator and router nodes. This established links between clusters of nodes shown in Fig. 11.

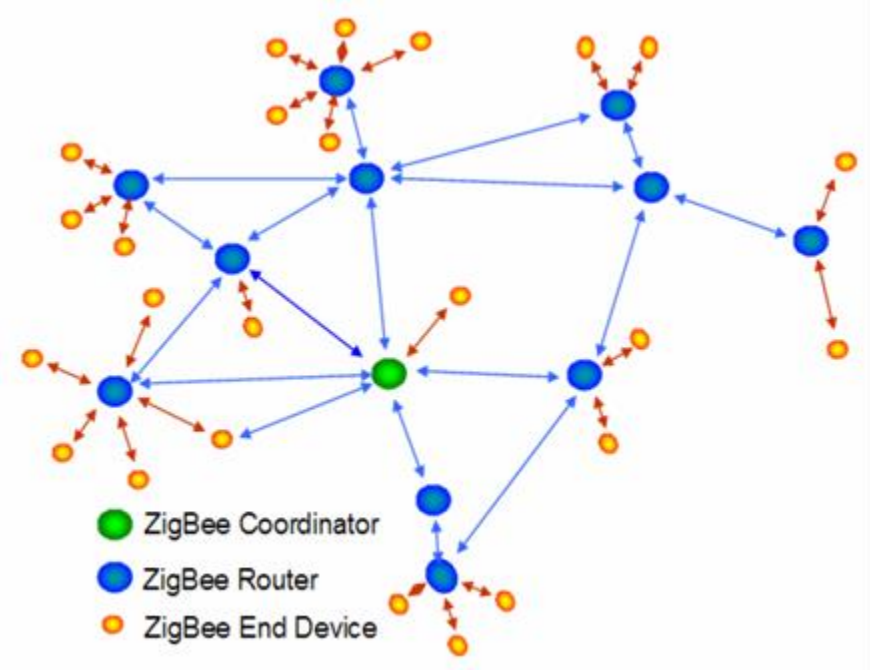

Figure 11: Wireless mesh network topology

Chapter 3: Microscopic Dust Sensor

3.1 Microscope Sensor Overview

Experimentation was done with using a digital microscope to determine dust-air concentration and to perhaps provide additional dust characteristics like particle color or size. Through experimentation it was discovered that dust particles in air move too quickly past the viewing window of a 500x magnification digital microscope. An industrial purposed high-budget camera could perform better, but due to project budget constraint it was not an option. A method was needed to slow the particles for long enough time to capture an image. One way to slow the particle would be to capture it in a liquid. Controlling the flow of the liquid would control the speed of the suspended particle.

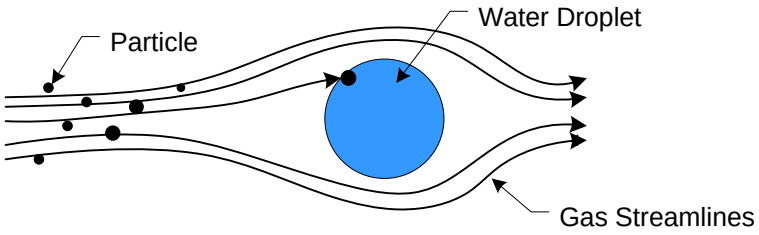

Figure 12: Impaction principle

Particles can enter a liquid through impaction as shown in Fig. 12. Impaction occurs when a particle physically collides with a liquid droplet. Two factors affect the probability of impactions occurring; the aerodynamic particle size, and the difference in velocity between the particle and the droplet. Larger particles are collected more easily in a droplet because of their inertia. Collection efficiency increases as the difference in velocity between the particle in air and the droplet increases.

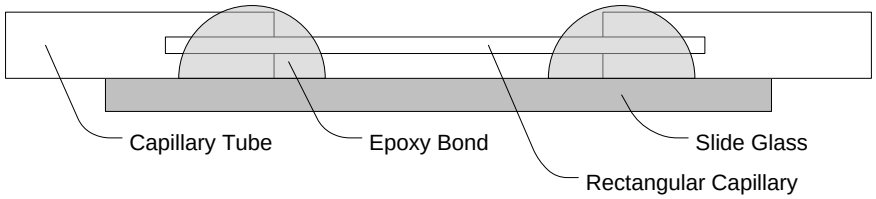

Figure 13: Custom microscope slide

Once the particles are suspended in a liquid then they can be pumped through the viewing area of the microscope. A custom microscope slide, shown in Fig. 13, was made based on a diagram from a paper on Particle Image Velocimetry (PIV) [22]. The principle is to create a microchannel using a rectangular glass capillary tube matching the width and depth of the microscope's viewing area. This would force every particle through the viewing area to allow the particle to be captured in an image.

Putting the ideas of collecting particle through impaction and capturing images using a microchannel together a new sensor design was constructed in Fig. 14. A prototype was fully built using micropumps, electronics, USB microscope, and miscellaneous materials. A full material BOM is shown in Appendix B.

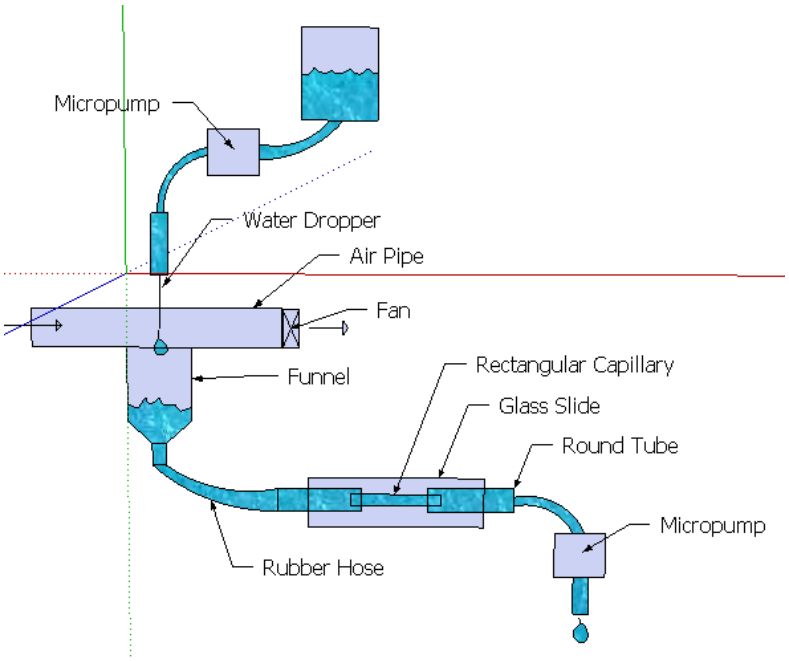

Figure 14: Microscope sensor components

3.2 Microscope Sensor Construction

The upper section of the microscope sensor consists of a liquid storage reservoir, a micropump and controller, tubing, and a needle. The micropump runs at a constant rate feeding the needle with liquid. The needle creates liquid droplets; the larger the diameter of the needle the larger the drops will become before falling into the funnel. The needle should be placed at a higher altitude than the reservoir so gravity does not make it flow uncontrolled.

The middle section of the microscope sensor combines the air stream containing dust particles with the liquid droplet through the method of impaction. A fan moves air across the liquid droplet at a constant rate. A funnel collects the droplets and has a liquid level sensor to provide a feedback signal to the second micropump.

The lower section of the sensor has a micropump that has two responsibilities. First it must evacuate the liquid from the funnel at the same rate as the droplets from the needle fill the funnel. The level is controlled using two flowrates and a liquid level sensor. When the liquid level sensor detects the liquid then a flow rate is used which is higher than the incoming rate of the needle dropper. When no liquid is sensed then a slower flowrate is used which is slower than the incoming rate of the liquid. This is a simple but effective control scheme that prevent overflow and prevent emptying the funnel which would cause air bubbles to enter the tube and possibly stall the micropump. The second responsibility of the lower micropump is to stop the flow of the liquid just long enough to take an image with the microscope. The microscope is carefully aligned above the rectangular capillary tube keeping it centered and in focus. Downstream from the microscope area the liquid flows into a collection reservoir. The collection reservoir is placed at a higher altitude than the funnel so gravity does not cause it to flow. A check valve is placed in-line with the tubing since some micropumps allow liquid to flow back into the funnel. The full sensor prototype used for image collection during chamber tests is shown in Fig. 15.

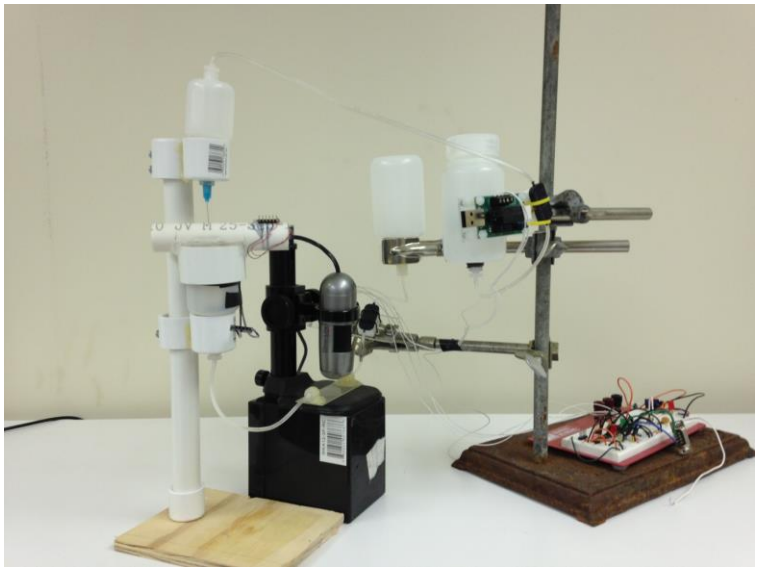

Figure 15: Microscope sensor prototype

The micropump in this sensor is a Bartels-Mikrotechnik MP6 which is a piezo actuated micropump for gases and liquids with a maximum flow rate of about 7 ml/min. Pump is driven by driver board (MP6-EVA or MP6-OEM) with 0-300Hz actuation frequency and 0-250V.

A Dino-Lite Pro USB microscope camera with 500x magnification was used. It can be treated like a webcam and easily interfaced to a software program to control image capturing. An accessory stand was purchased to facilitate mounting and adjustment of the microscope relative to the capillary slide. The camera specs are shown in Table 1.

Table 1: Microscope Sensor Specifications

Model	AM413MT5 Dino-Lite Pro
Magnification	500X Fixed
Pixels	1.3M
Resolution	1280x1024
Sensor	Enhanced Color CMOS
Data Output	USB 2.0

3.3 Software Design

A simple software program, shown in Fig. 16, was created to time the collection of microscope images from the sensor during operation. It allows for adjustment of the image capture frequency and the delay from when the pumps are stopped and the image is captured. This timing was determined experimentally so that the dust particles are no longer in motion when the image is captured.

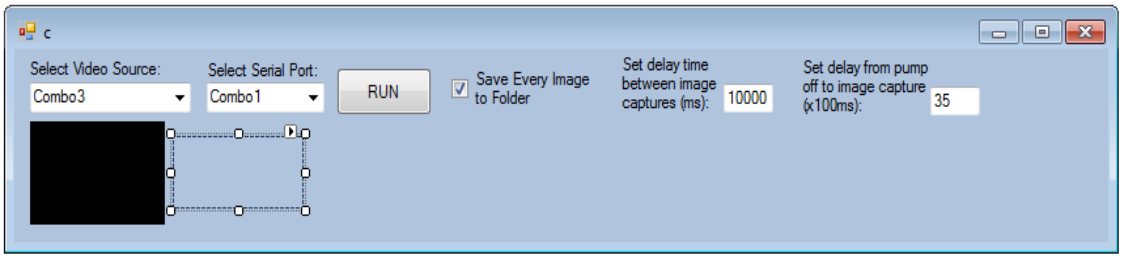

Figure 16: Image collection software

The software program connects to the camera and has a serial data connection to a Microchip PIC microcontroller that controls the sensor. Clicking the RUN button starts

the operation of the microscope portion of the sensor saving jpeg images of resolution 1280x1024 (1.3M pixel) to hard disk. The delay time between image captures is sent to the microcontroller. When the microcontroller timer expires it sends a message to the software telling it to capture an image. Three consecutive images are captured at a rate of 30 frames-per-second at every pause of the pumps. The live image is displayed in the software window for real-time viewing.

Between images the microcontroller controls the pump rate of the lower pump. It keeps the liquid level in the collection funnel constant. Figure 17 shows the control logic and program flow.

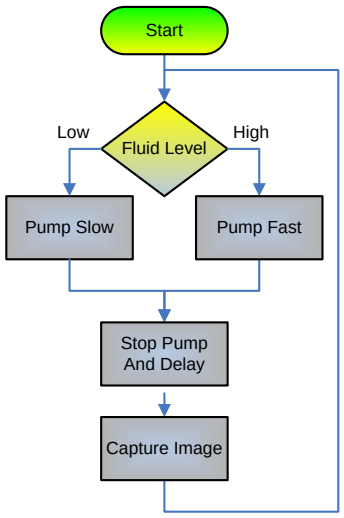

Figure 17: Sensor control logic

3.4 Image Processing Algorithm

A separate software program was created to process the collected images from chamber testing. The program runs an algorithm to detect dust particles and calculate particle size and mass. To begin, the images are converted to grey scale. A running average of ten images is maintained as a saved image representing the image background. Each image processed has the background subtracted from it; the dust particles show as brighter pixels than the background because of the camera lighting. If a subtraction happens to be a negative result then the pixel is set to a value of ‘0’ representing a black pixel.

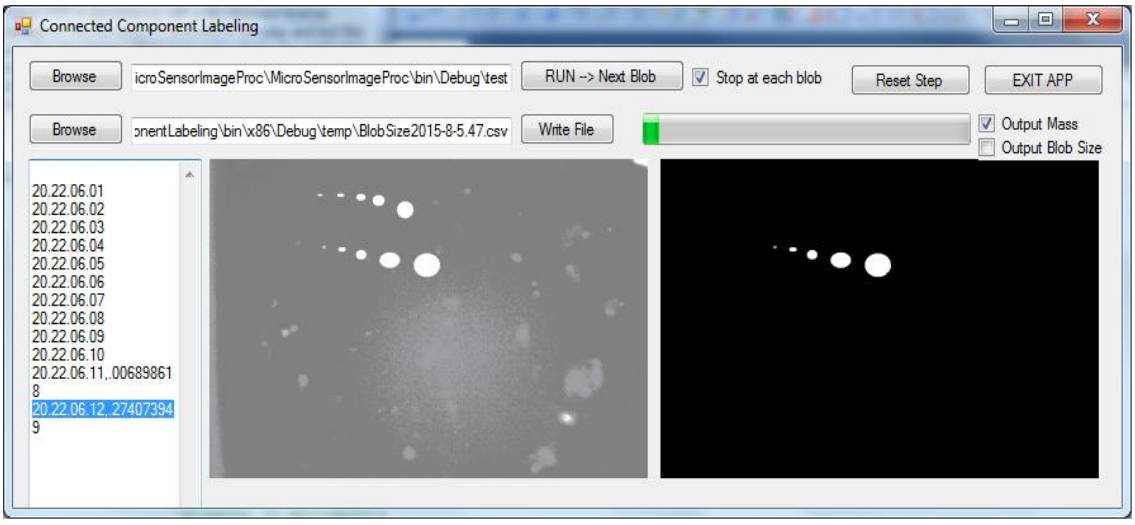

Figure 18: Background subtraction and threshold test image

Next a histogram is run on the images counting the number of pixels at each value ranging from 0 (black) to 255 (white). The histogram is used to choose the threshold used to convert all pixels to black if their grey value is below the threshold, or white if their value is above the threshold. The result is a black and white image as in Fig. 18. Plotting the histogram values on a LOG scale in Fig. 19 shows the majority of the pixels are black.

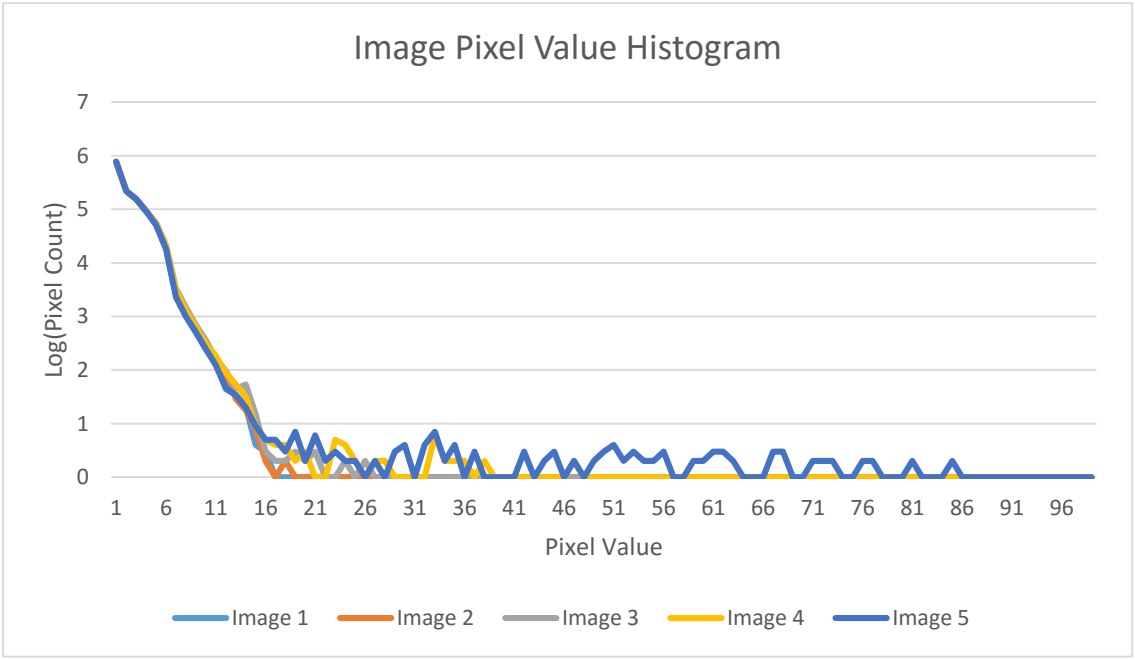

Figure 19: Image pixel value histogram

The method to determine the threshold value (0-255) uses a percentage value representing the percent of total pixels that are black. The pixels are summed starting at the number of pixels with value 0, plus the pixels with value 1, and so on until the pixel count reaches this percentage of total pixels. The percentage constant was determined experimentally by viewing the resulting images as various setting and found to be 99%. The value is consistent from test to test due to well controlled lighting and background and similar concentration of dust particles.

The black and white image after this processing shows the white dust particle clearly along with salt and pepper pixel noise. A median filter with a neighborhood of 3x3 pixels is run next to reduce this noise. Other filters were tried but the median filter by experimentation proved effective.

3.5 Connected Component Labeling

Next each pixel must be identified as its own entity. A connected-component labeling (CCL) algorithm was coded from scratch. CCL is an algorithmic application of graph theory where subsets of connected components are uniquely labeled based on a given heuristic [23]. It is used in computer vision to detect connected regions leading to region labeling also known as blob detection. A blob is defined as a region of a digital image with properties such as brightness or color that vary within a prescribed range of values. In this case a blob refers to the detection of a dust particle in the image.

CCL is a two-pass algorithm. The first pass traverses the pixels left-to-right then top-to-bottom assigning temporary labels to white pixels. The second pass records equivalencies (the same blob) and replaces each temporary label with the smallest equivalent label. Conditions to check in the first pass are:

Does the label to the West have the same value as the current pixel?

Yes – They are in the same region, assign the same label to current pixel

No – Check the next condition

Does the label to the North have the same value as the current pixel?

Yes – They are in the same region, assign the same label to current pixel

No – Check the next condition

Does the label to the North-West have the same value as the current pixel?

Yes – They are in the same region, assign the same label to current pixel

No – Check the next condition

Does the label to the North-East have the same value as the current pixel?

Yes – They are in the same region, assign the same label to current pixel

No – Check the next condition

Else do not assign a label to current pixel

Figure 20 shows the current pixel in the center in pink, and the searched pixels from the above algorithm. The method continues through the entire image and assigns new labels when needed.

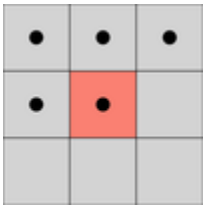

Figure 20: Connected Component Labeling search pattern

An equivalency table is generated creating a new Set ID when there are no neighbors greater than zero value. When a neighbor has a value greater than zero it is added to the Set ID of the current pixel. An example Set ID list for a demonstration image is shown in Table 2.

Table 2: CCL Equivalency Table

Set ID	Equivalent Labels
1	1,2
2	1,2
3	3,4,5,6,7
4	3,4,5,6,7
5	3,4,5,6,7
6	3,4,5,6,7
7	3,4,5,6,7

The next step in the CCL algorithm is flooding the regions with the smallest equivalent label. Assigning a color to each unique flooded region identifies the separate

blobs. Several test arrays were used as simulated image data to test the software. Figure 21 displays the test arrays in the final two steps of the CCL algorithm.

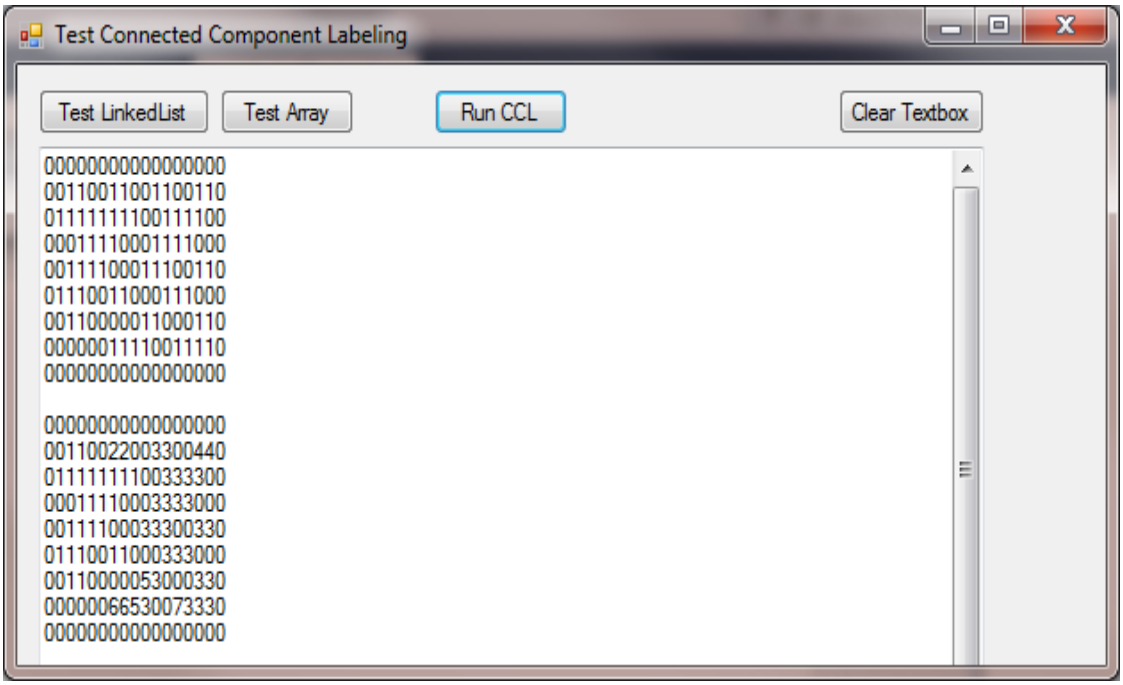

Figure 21: Initial testing of the CCL algorithm on simulated data

3.6 Particle Sizing

There are many existing methods to characterize the size or diameter of a particle that is not a perfect sphere. The method chosen for this software was Equal Area Projection. This is the diameter of a circle with the same area as the area of the pixels taken up by the particle. To accomplish this the total number of pixels in a blob are counted and converted to an area in square micrometers, and then a diameter of a circle of equal area is calculated.

The scaling of pixel size to micrometers is found by capturing an image of a micrometer calibration scale that is designed for microscopes. When zoomed in on the scale, the individual pixels could be differentiated from their neighbors. The count of micrometer scale lines divided by the number of full pixels resulted in 0.7704 micrometers per pixel.

$$A = \pi r^2 \qquad (3)$$

In Eq. (3), ‘A’ is the Area in square pixels obtained from the pixel count of the particle blob. Solving for ‘r’ yields:

$$r = \sqrt{A/\pi} \tag{4}$$

Where r is the radius of the particle with units still in pixels. Converting radius to diameter in micrometers:

$$d = 2(0.7704)\sqrt{A/\pi} \tag{5}$$

To get mass of the particle from its diameter, the mass equation for a sphere Eq. (6) is used:

$$m = \frac{\pi}{6}\rho d^3 \tag{6}$$

Where ‘m’ is mass, ‘ρ’ is the density of the particle, and ‘d’ is the diameter. The density for the manure sample tested here was 1.8 g/cm³. Converting the mass equation to use diameter in micrometers and to get mass in micrograms, Eq. (7) is used:

$$m(\mu g) = \frac{0.3\pi d^3}{1x10^6} \tag{7}$$

The image processing software has an option checkbox to allow the user to output each particle diameter or total particle mass for each image.

Chapter 4: Dust Chamber Design for Sensor Testing

4.1 Hardware Introduction

A dust generation chamber was needed to assist in the design of an optical dust sensor offering the ability to run tests in a convenient and timely way, and to assist in the calibration of the sensors and comparison to a commercial sensor. A paper was published by this researcher entitled “Development of Low-Cost Dust Generation Chamber and Wireless Nephelometers for a Feedlot Dust Study” and a poster presented at the International Symposium on Air Quality and Manure Management for Agriculture (ASABE) on September 2010. The following sections will explain the hardware design and design considerations of the dust generation chamber.

4.2 Dust generation chamber

A dust generation system (DGS) was needed to test the detection range of our new nephelometer sensor and also to calibrate the sensor. Purchasing commercial dust generation equipment was not within the project budget. Instead, a low cost, dust generating environment that produces a high degree of dust density variations was constructed from COTS (commercial off-the-shelf) components for about $245 (see DGS Bill of Material in Appendix C).

Three classifications of dust generators exist [21]. These are (I) fluidization, (II) gravitation, and (III) mechanical dispersion or agitation. A type-III dust generator can be built by modifying a kitchen blender. Dust generation is also classified under two additional headings: puff or cloud. The kitchen blender implements the cloud method where a large amount of dust is generated and a small representative portion of dust is sampled by the sensors.

This dust generation chamber consists of three systems: the intake/dust generation, the settling/sampling chamber, and exhaust/dust collection. Figure 22 shows the DGS system.

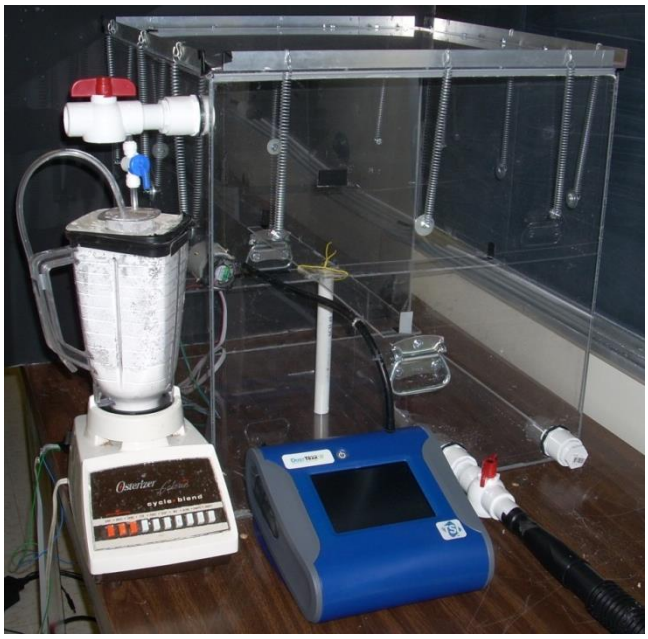

Figure 22: Dust generation and sampling system

4.2.1 DGS Operation

The dust generation of the DGS system in Fig. 23 is responsible for creating a dust aerosol and mixing it with fresh air. The kitchen blender produces dust by mechanical agitation of a dust sample. The dust is carried up into the dust feedline (F) by the system vacuum. A breather hose (G) is installed to replace the evacuated air and also to help the dust move upward into the feedline. A baffle (I) is placed in the blender to help keep large debris down near the blades while allowing small airborne particles to float up to the top through a hole in its center. A valve on the feedline tube allows the user to adjust the flow rate from the dust generator. This valve is one of several means of controlling the dust concentration.

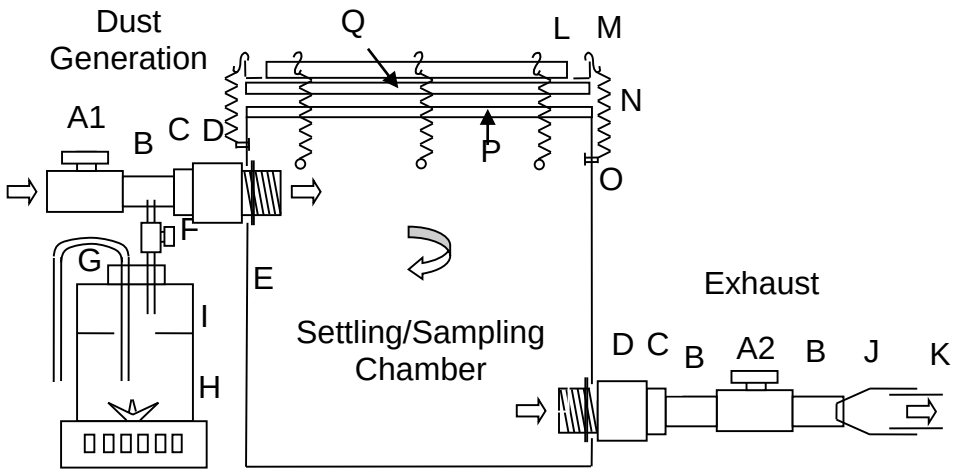

Figure 23: Dust generation system diagram

A valve (A1) is placed at the inlet of the intake. This valve can be closed slightly if it is necessary to increase the flow in the dust feedline and increase the dust concentration. The aerosol dust from the feedline is combined with fresh air in a pipe (B) and then enters the chamber through two adapters (C,D). A filter can be added to the intake to ensure clean air enters the system.

The settling/sampling chamber provides a specified volume in which the dust can mix and ideally become more uniform in concentration while providing a lower air velocity. It also provides a location for mounting sensors and to sample a representative portion of the dust. The top is clamped on using springs so it can easily be removed for cleaning. The intake is placed near the top of the chamber and the exhaust near the bottom. This is because gravitation effects on the dust cause it to accumulate near the bottom.

The chamber exhausts through a valve (A2) and into a shop vacuum (K). The vacuum is the motive force that moves the air. The vacuum valve (A2) in the exhaust controls the rate air moves through the system. Opening the valve (A2) increases air flow which increases the dust concentration. The exhaust also collects the dust expelled by the system onto a filter.

4.2.2 Construction Detail

The DGS is constructed from COTS components such as a kitchen blender, PVC piping and fittings, 1/8" acrylic sheeting, and a shop vacuum. Purchasing these items and assembling them based on the following procedures should create a DGS with identical characteristics.

4.2.2.1 Intake

The kitchen blender (H), shown in Fig. 24, agitates the sample. The blender cap is installed and sealed with an all-purpose silicone rubber. A baffle (I) is fitted about 2" from the top of the blender. The baffle is made from the same 1/8" acrylic sheet as the sampling chamber (E). The baffle is cut to fit to the inside of the blender and is taped into place so it can be removed for cleaning. A 1" hole is drilled in the center of the baffle for the dust aerosol to flow upward.

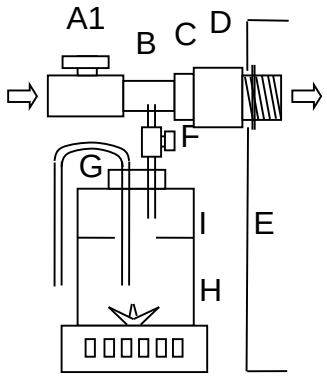

Figure 24: Intake components

Two 1/4" vinyl tubes enter the blender through two holes drilled in the cap. One is the dust feedline that connects the blender to the intake pipe. The other tube (G) acts as a breather hose allowing air to enter equalizing pressure and also helps the aerosol generated near the mixing blades flow upward toward the dust feedline. The dust feedline carries the concentrated dust mixture from the blender to the chamber intake. A 1/8" I.D. valve (F) is placed in the feedline. The feedline enters the intake through a 1/4" hole drilled in a section of 3/4" PVC pipe (B).

The intake system starts with a 3/4" PVC valve (A) and connects to a 3" section of 3/4" PVC pipe (B). This connects to a 3/4" to 1" PVC bushing (C) and then into a 1"

PVC adapter with fastening nut (D). A rubber washer with nut fastens and seals the intake to a 1-3/8" hole drilled in the settling chamber (E). The mounting height of the intake system on the sampling chamber can be adjusted according to the height of the kitchen blender so they both sit on the same table surface.

4.2.2.2 Settling and Sampling Chamber

The settling chamber in Fig. 25 is assembled into a box from pieces cut from a 4'x8'x1/8" sheet of acrylic (E). The box is cut and glued to form a 20" cube with a volume of 8000 cubic inches (0.1311 m^3). The length of each side of the chamber is properly adjusted for edge overlap to give 20" on the inside-to-inside measurement. The acrylic can be cut on a table saw and fastened together using an acrylic bonding agent.

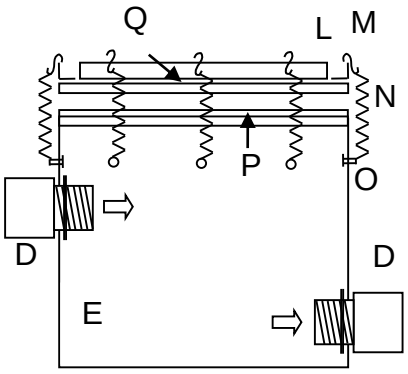

Figure 25: Settling/sampling chamber components

Vinyl weather-stripping (P) is glued around the perimeter of the box to form a tight seal against the top. The top of the box (Q) is cut 1” larger than the bottom to give enough area for the seal. Aluminum angle-iron (L) is then bolted around the top edges to attach the springs and help to disperse the spring force. Three small 1"x1/4" bolts (O) are placed in each side through drilled holes about 7" down from the top. Springs (N) are placed around the circumference to tightly hold the top in place. S-hooks (M) are placed on one end of the springs to attach them to the top angle-iron while the loop on the other end is simply hooks around the small bolts (O).

The 1" PVC adapters (D) for the intake and exhaust ports are bolted onto the chamber through 1-3/8" holes. A retaining nut and rubber washer are included with the drain to clamp and seal it to the chamber wall.

A cross brace can be made from the acrylic to reinforce the center of the chamber walls. This is shown in Fig. 1. Simply glue two 2"x20" acrylic strips at the center. A short piece of PVC pipe can be cut to hold the cross at a specific height. Taping the cross to the chamber walls allows it to be easily removed for cleaning the chamber.

4.2.2.3 Exhaust and Dust Collection

The exhaust construction, shown in Fig. 26, is very similar to that of the intake. A 1" PVC adapter with fastening nut (D) is attached to a hole in the chamber wall (E). A 1" to 3/4" PVC bushing (C) connects a 3" section of 3/4" PVC piping (B). The pipe is then attached to a 3/4" PVC valve (A2) and then back to another section of pipe. A vacuum attachment (J) reduces the vacuum hose (K) to fit inside the PVC pipe. It is secured with tape. A collection filter can be placed either in the shop vacuum or as its own module between the vacuum and the exhaust.

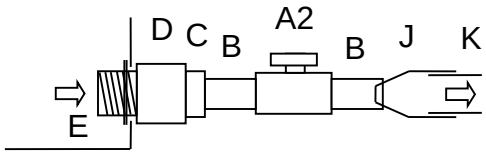

Figure 26: Exhaust components

Chapter 5: Experimental Results

5.1 Calibration Procedure for Nephelometer

Working on a limited budget prevents the purchase of professional equipment. A dust generator purchased from a distributor costs around $18,500 which would consume a majority of the project's budget. It would produce a very accurate aerosol output with easy concentration adjustment. It is difficult to construct a dust generator of high accuracy given the project budget and available man-hours; it is no trivial matter. Complex research has been conducted in that field alone.

The calibration of this nephelometer sensor was performed in a home-made dust generation chamber. The chamber consists of a kitchen blender to agitate the dust sample, a 20 inch cube acrylic box for the introduction of the dust to the sensor, and a shop vacuum to force the air through the system. The chamber can generate a wide range of dust concentrations. Only 16 mg/m³ peak concentration was required for this calibration and the dust chamber easily provides this.

Feedlot manure that had been run through a cyclone to separate larger particles was the dust sample material used for calibration. This material was placed in the blender. The sensor was placed in the 20 inch cube chamber near one wall and centered vertically. A DustTrak™ II 8530 Aerosol Monitor was used as the reference sensor for calibration. Its range was set for 0 to 16 mg/m³. The DustTrak produces an analog output of 0 to 5V for the range selected. This voltage is sampled and converted to concentration in mg/m³ by custom made circuit board and the data is sent wirelessly to the data logger. The inlet tube for this sensor entered the chamber and terminated next to the inlet of the dust sensor to be calibrated.

The shop vacuum is turned on for a few minutes until it is warmed up. Then both sensors are turned on to begin sampling dust concentrations. Next, the blender is turned on, and a valve in the tube from the blender to the chamber inlet is opened. The valve is opened enough to bring the concentration up to 16 mg/m³ and then is fully closed, allowing the dust to dissipate from the chamber. The vacuum continues to run until the dust level drops to near zero, after which the data collection is finished.

The data is then imported in Microsoft Excel for analysis. The data is adjusted so that the time stamps of both sensors are aligned. Next, the DustTrak data must be time-shifted to account for the three-second delay resulting from the dust travel time through the sample tube. The result of these data operations is shown in Fig. 27.

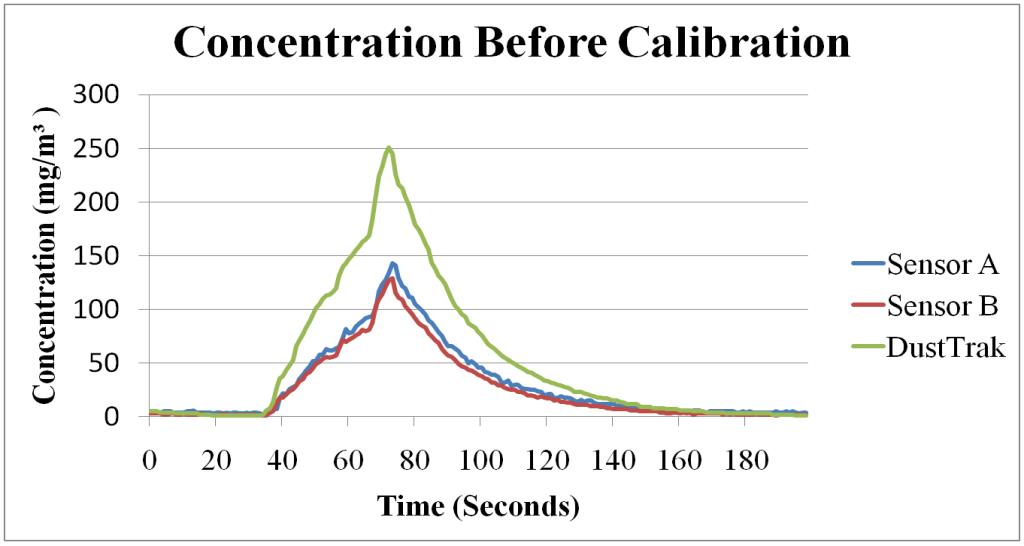

Figure 27: Nephelometer data pre-calibration

The dust concentration measurements are smoother on the dissipation side of the curve as opposed to the more erratic measurements on the dust injection side of the curve. The dissipation data is isolated for use in calculating the calibration factors. The sample data, up to 3 samples after the last peak value of the three sensors, is discarded from the calculations. This isolated portion of the data is shown in Fig. 28.

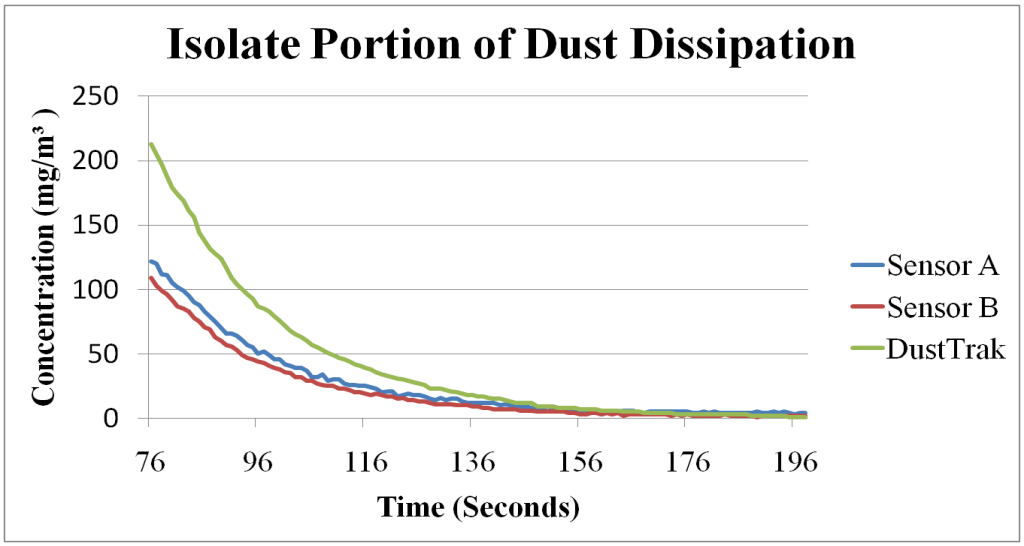

Figure 28: Isolating tail portion of nephelometer data

Next, each sensor is plotted against the DustTrak data to fit a linear regression line. An equation is given by Excel from the regression line (Fig. 29) that will be used for the sensor calibration. It is a slope-intercept equation in the form of "y = mx + b".

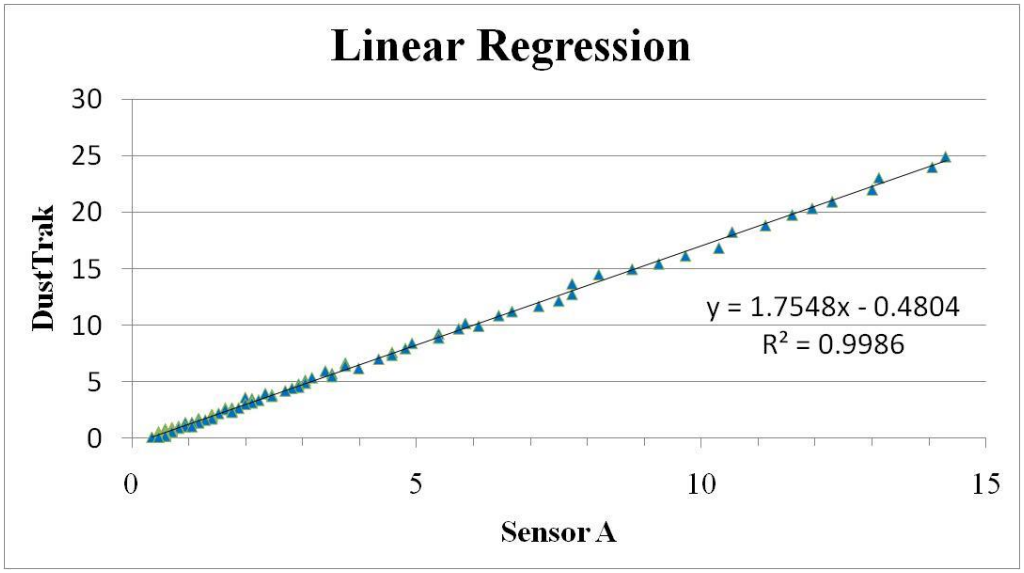

Figure 29: Performing linear regression of nephelometer data

The number in place of "m" in this equation is the scale factor (M) that is entered in the sensor menu calibration settings. Similarly, the number in place of "b" in this equation is entered as the y-intercept (B) parameter. These numbers are rounded to the

hundredths decimal place. The 16 mg/m³ peak setting of the DustTrak is set as the Peak (P) parameter in the sensor menu. The sensor is now calibrated after making these entries. Applying these calibrations to the data from the test yields the result shown in Fig. 30.

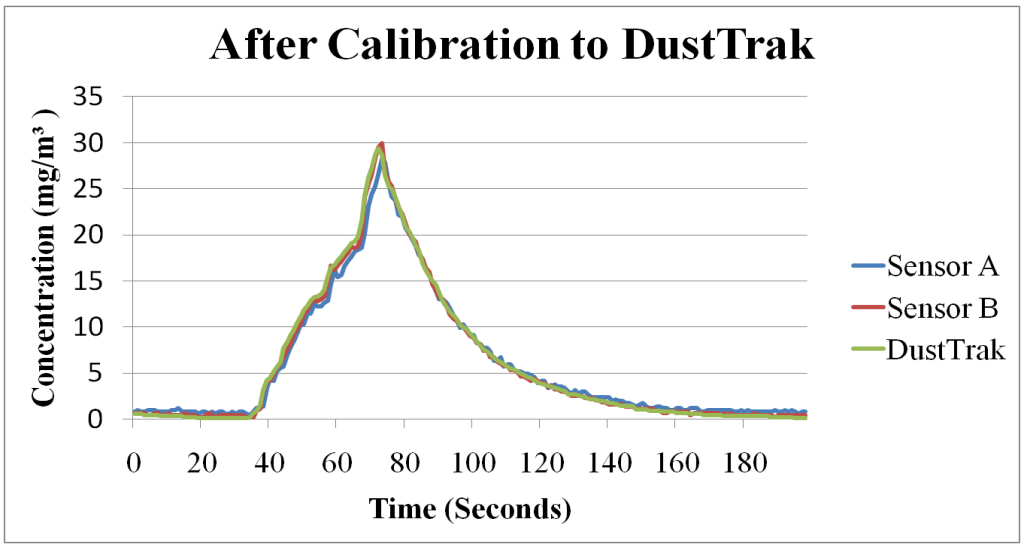

Figure 30: Nephelometer calibration results

5.2 Nephelometer Field Test

In February 2011 the first field test of the Nephelometer sensors was performed. It was at a cattle feedlot near Amarillo Texas. There was snow in the week previous to testing so there was not maximum evening dust peaks during the testing duration. Figure 31 shows the sensor placement around the reference TEOM sensors. The reference TEOM sensors average data never went above 0.2 mg/m3. This concentration is only in the first 1.25% of the nephelometer's range so the data does not lead to any substantial conclusions.

Figure 31: Nephelometer field test at a Texas feedlot

In June of 2011 there was a field test performed by the University of Texas A&M AgriLife research team under the direction of Brent Auvermann Ph.D. with ten nephelometer sensors along with one TEOM reference sensor. This test condition was among a typical worst case evening dust peak for this feedlot. The test period was about 22 hours. Figure 32 shows the sensor data through the entire test duration. All the sensors trend well to the TEOM data, but there is an obvious residual effect after the evening dust peak. The concentration values do not return back to a low concentration value, instead they hold some steady state offset. This is likely due to some dust accumulation on the optics. Even with the accumulation of dust on the optics, the sensors still trend well to variations in dust levels.

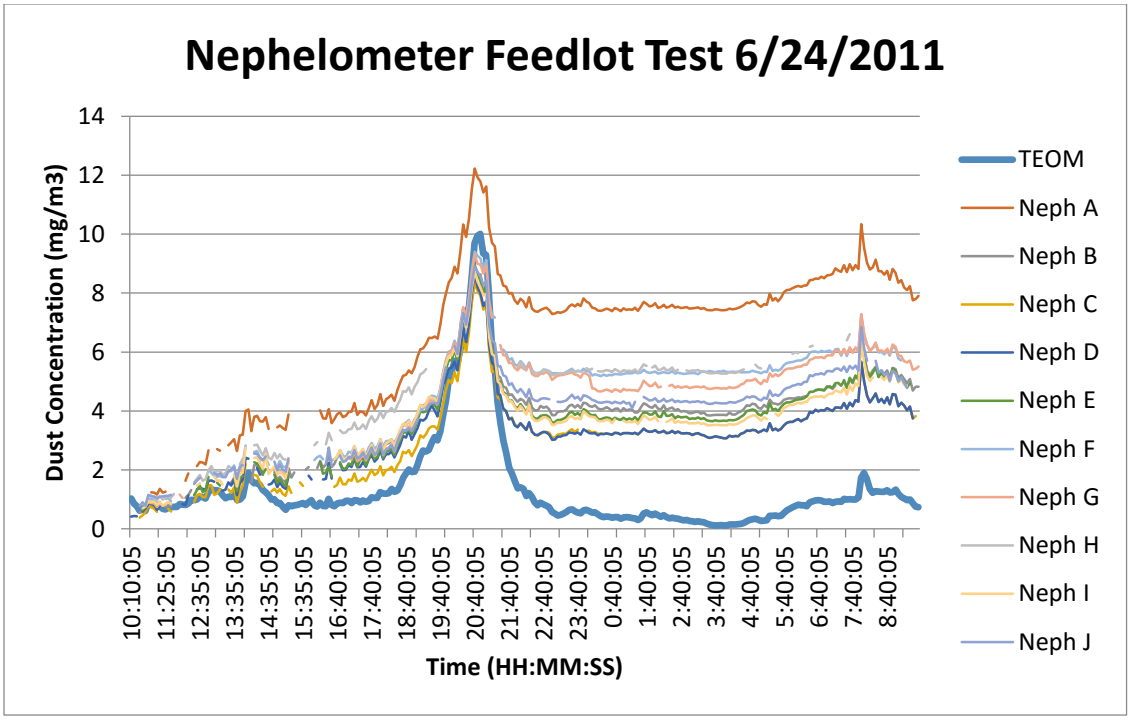

Figure 32: Nephelometer field test data

Figure 33 shows the average of the Nephelometer sensors A through J versus the reference TEOM sensor. The graph clearly shows a residual effect at low concentrations of the dust accumulating on the sensor optics.

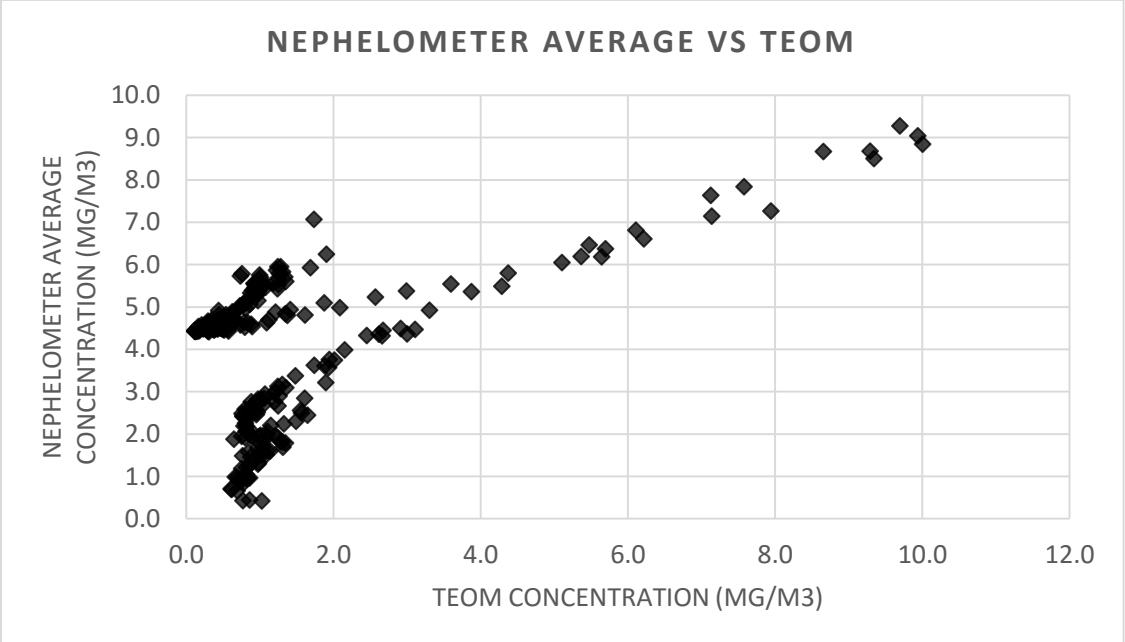

Figure 33: Nephelometer residual effect

Table 3: Nephelometer Standard Deviation

Average Standard Deviation	1.03
Max Standard Deviation	1.65
Min Standard Deviation	0.08

The standard deviation of sensors A through J is shown in the Table 3. The root-mean-square-error (RMSE) is also calculated using the average Nephelometer data and the TEOM data. The RMSE from the test start to halfway to the evening peak was the lowest at 0.77 mg/m³. At this point there was not much dust accumulation on the optics. From the halfway point to the evening peak the RMSE was much larger at 2.98 mg/m³. It held approximately this error through the end of the test because there were no more large dust peaks to dirty the optics. The residual effect of the dust on the optics only allows the error to grow lightly through the portion of the test after the dust peak yielding an overall RMSE of 3.10 mg/m³. These values are summarized in Table 4.

Table 4: RMSE Calculation for Nephelometer and TEOM Data

RMSE 10:10:00-15:15:00 (Pre-Peak)	0.77
RMSE 15:15:00-20:40:00 (Peak)	2.98
RMSE 20:40:00-9:35:00 (Post-Peak)	3.23
RMSE 10:10:00-9:35:00 (Entire Test)	3.10

5.3 Microscope Sensor Lab Test

A data set of microscope images was collected by running the DGS chamber for ten cycles of high concentration dust ranging from 0 to 30 mg/m³ and eight tests of low concentration dust below 1 mg/m³. Each test consisted of injecting dust until the desired peak concentration was seen on the live readout of the DustTrak reference sensor, and then letting the dust settle and exit the chamber for several minutes. Images for each dust cycle were stored on disc to be processed at a later time.

A series of images is shown in Fig. 34 at various stages of processing. Image (1) is the image capture by the sensor. Image (2) is after subtracting the average background. The LED light on the camera provided consistent lighting so the background was very consistent. Subtracting the background removes most of the image that is not of interest. Image (3) applies the thresholding turning all values below the threshold black and all pixel values above the threshold white. Lastly, a median filter was applied to clean up the salt and pepper pixels that are not dust particles shown in image (4). At this point the connected component labeling algorithm identifies each dust particle as its own blob and the blob sizes are determined using the method of equal area projection. This blob diameter is then used along with particle density to calculate the particle mass.

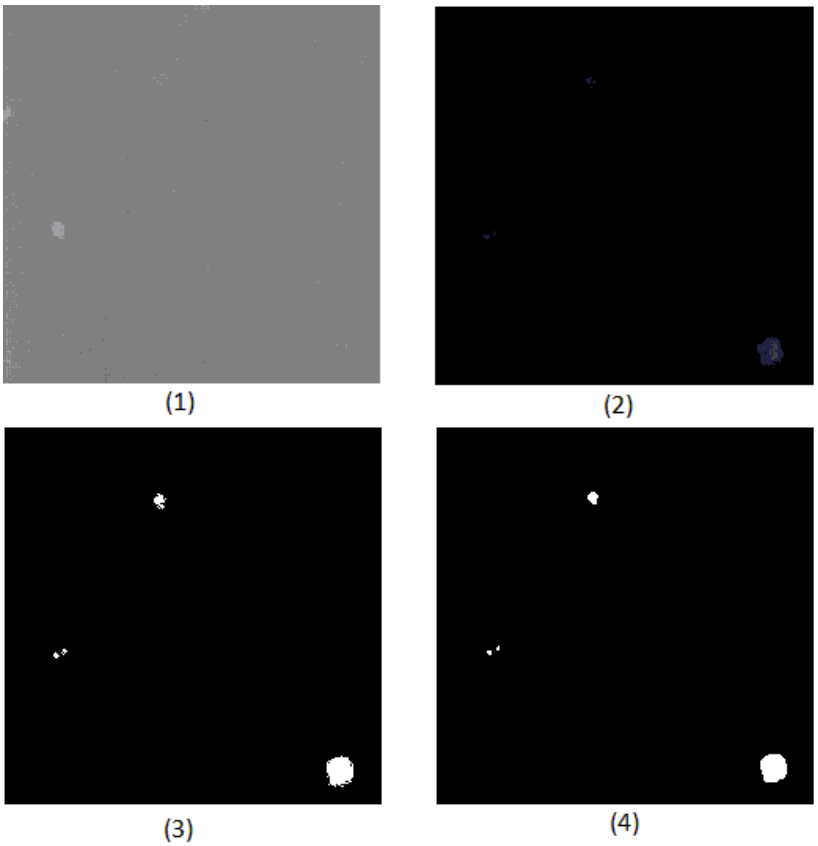

Figure 34: Image pixel value histogram

Image processing software was run on all of the image data sets. The output was a CSV file of calculated particle mass in micrograms.

The comparison of the microscope sensor and the DustTrak sensor can be seen in Fig. 35. The DustTrak recorded distinct high-concentration periods accurately showing each test cycle. The microscope sensor is not as distinct. It detects particles but does not appear to be as cyclic as the DustTrak data.

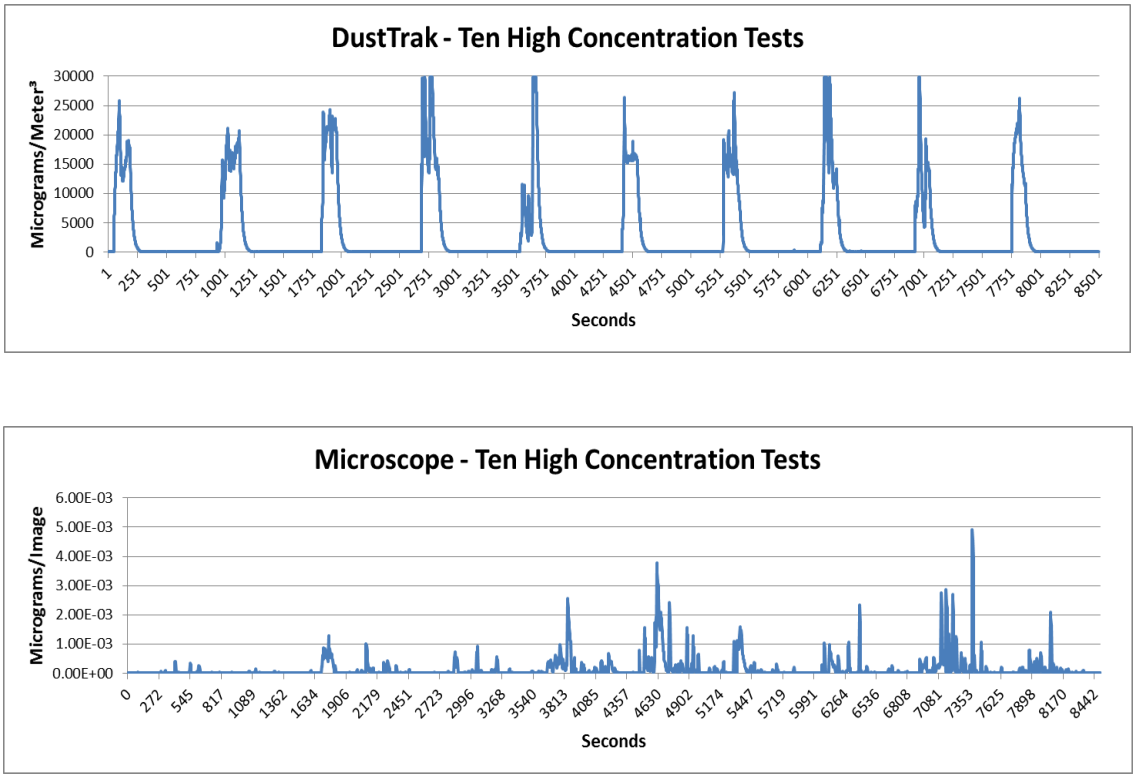

Figure 35: Microscope sensor and DustTrak measurements

The data can also be viewed as mass accumulation. Integrating the concentration data over time yields mass in micrograms. In Fig. 36, both sensors are plotted in mass vs. time and both are normalized to 1.0 by dividing all values by the maximum value.

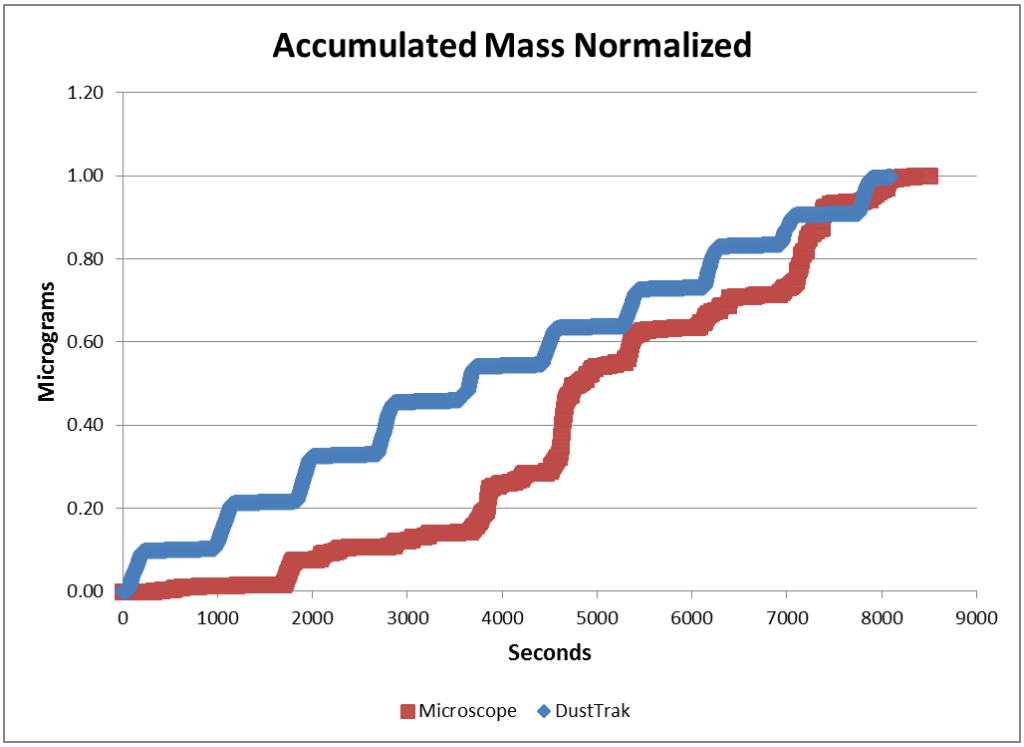

Figure 36: Microscope sensor accumulated mass

The microscope sensor was not as real-time as the DustTrak; it had time delay due to the time it took the dust particle to travel to the microscope slide from the sampling area. The microscope sensor data does trend similarly to the reference sensor data with a maximum error of about 33%. The error usually underestimates the reference sensor. This could be explained by the low particle capture efficiency at the sampling area combined with the possibility of missing images of particles due to the low image capture rate which is an image every 3 seconds.

Chapter 6: Air Dispersion Modeling for Evaluation

Air dispersion modeling is an attempt to obtain a relationship between pollution emissions, occurring concentrations, and deposition and how air pollutants disperse in the atmosphere. It can be used to predict the air concentration downwind from an emission source and to help plan air pollution control programs. It's used for assessing environmental impact and to determine the benefits of pollution abatement methods.

An air dispersion model is a mathematical relationship between emissions and air quality that incorporates the transport, dispersion, and transformation of the pollutants in the air. The concentration of air pollution is typically measured downwind from a source. Variables that affect concentration are the amount of pollutant release from the source, the distance the sensor is from the source, and the atmospheric conditions such as wind speed and direction, and temperature over a vertical distance.

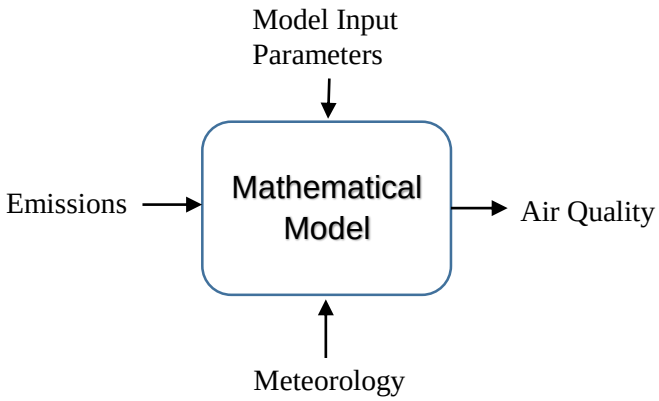

Figure 37: Air pollution model basic parameters

Models like Fig. 37 can never completely replicate a system, but are useful for characterizing an environment. It may have several input parameters to increase the accuracy of the output. Often times if the input parameters are not well known to be accurate then the model will not be very accurate. Simple models do not rely on complicated input parameters.

6.1 Box Model

The box model is commonly used because it is the simplest of the model types. The airshed is represented by a box over the dust emission site with some height, length, and width. One end of the box is placed at the downwind direction. The wind carries the dust along the box. The box model equation calculates the average dust concentration anywhere within the box.

The model maintains its simplicity due to some assumptions. It assumes: the box has sides, lid, and flat bottom at ground level, the dust inside the box is a homogeneous distribution, the plume from the emission source has expanded to include the entire area of the box, one side of the box is parallel to the wind direction, that no dust exits the top or sides of the box, and steady state emissions and atmospheric conditions.

As with other models, the box model uses a material mass balance approach:

Accumulation rate=All flow rates in – All flow rates out + creation rate – destruction rate

The box model depicted in Fig. 38 only uses flow rates in and out of the box and sets the creation, destruction, and accumulation rate terms to zero.

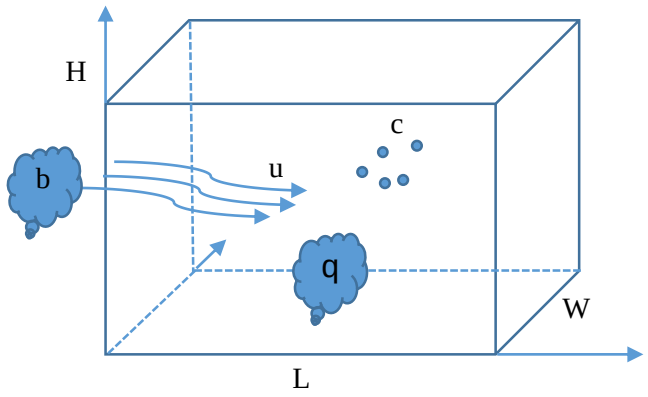

Figure 38: The Box Model parameters

The box model is used to derive Eq. (8) calculating the concentration in the box. Definitions for parameters in the box model:

b: upwind concentration ug/m³

u: wind speed m/s

q: emission rate within box ug/s/m²

c: concentration in the box ug/m³

W,L,H: Width, Length, Height of the box in meters

Derivation:

0 = Flow rate in - flow rate out

Flow rate in upwind side, uWHb = (volume/time) x (mass/volume) = mass/time

Flow rate in emitted inside box, qWL

Flow rate out, uWHc

Substituting:

0 = (uWHb + qWL) – uWHc

0 = W(uHb + qL – uHc)

uHc = uHb + qL

$$c = \mathrm{b} + (\mathrm{qL}/\mathrm{uH}) \tag{8}$$

A feedlot analysis using the box model solves the equation for emission rate to find the emission rate of the feedlot area [26]. The analysis states the concentration in the box, c, is the difference in concentration measured at the upwind and downwind ends of the box: C = (c-b). Substituting this into Eq. (8) and solving for emission rate q yields Eq. (9).

$$q = \frac{uHC}{L} \tag{9}$$

To estimate non-steady state condition an average concentration can be calculated by summing the concentration from one meteorology multiplied by its frequency [25,27]:

$$\text{Annual Concentration} = \sum_{all\ meteorologies}^{n} (\text{Conc for each meteorology}) * (Frequency\ of\ occurrence)$$

6.2 Gaussian Model

The Gaussian model (sometimes called diffusion model or dispersion model) is one of the most commonly used model types. It assumes that the dust concentration downwind from the source is a Gaussian distribution, or normal probability distribution. It can estimate the dispersion of a dust plume from a ground level source. The model can

be adapted to estimate both continuous and non-continuous dust plumes. Like the box model it is a material balance model. It can be used to describe the plume in one, two, or three dimensions.

To use the equation some assumptions must be made. It is assumed the plume spread has a normal distribution. The emission rate is constant and wind speed and direction is uniform and that the terrain is flat. For the portion of the plume that projects into the ground the model reflects that back upwards and it is assumed that none of the dust has resettled back to the Earth.

The coordinate system (Fig. 39) is modeled after a smokestack application. The origin is located at the base of the stack.

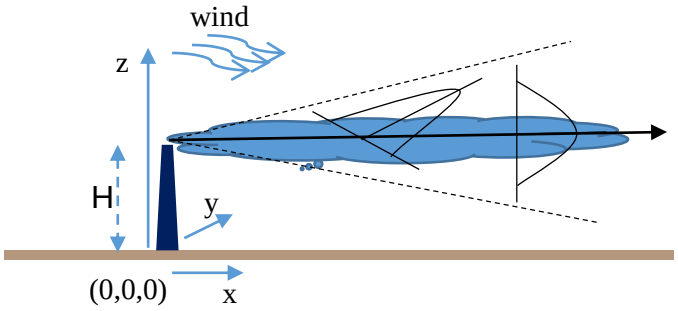

Figure 39: Coordinate system and representation of Gaussian Model

The coordinate system origin is at the base of the smokestack with the x-axis aligned with the downwind direction. The pollution rises (delta H) and travels downwind and spreads in the y and z directions as it travels. The y direction is perpendicular to the wind direction and parallel to the ground. Emission rate is Q in grams per second. The wind velocity is u in meters per second. Equation (10) calculates the concentration at any point in a 2-dimension system:

$$c = \frac{Q}{2\pi u \sigma_y \sigma_z} exp - \left[\frac{y^2}{2\sigma_y^2} + \frac{(z-H)^2}{2\sigma_z^2}\right] \qquad (10)$$

Parameters $\sigma_y$and $\sigma_z$are called horizontal and vertical dispersion coefficients with units usually in meters. The first term is the concentration on the centerline of the plume. In the exponential terms, the two values increase with downwind distance, so overall, the

centerline concentrations decrease with the downwind distance. The second and third terms show how the concentration decreases as we move horizontally and vertically.

6.2.1 The Effects of the Ground on the Gaussian Model

Most concern of dust plume is for near ground locations since that is where people and property are. In the above model the pollutants continue to disperse along the z-axis. Pollutants cannot penetrate the ground so they are reflected upward. To calculate this reflection an additional term $(z+H)^2$ is added that provides this mirror image in Eq. (11).

$$c = \frac{Q}{2\pi u \sigma_y \sigma_z} exp - 0.5\left(\frac{y}{\sigma_y}\right)^2 \left[exp - 0.5\left(\frac{z-H}{\sigma_z}\right)^2 + exp - 0.5\left(\frac{z+H}{\sigma_z}\right)^2\right] \quad (11)$$

Equation (12) is the most widely used estimating equation because it applies the greatest practical interest. It uses the reflected concentration from the ground and sets z=0.

$$c = \frac{Q}{\pi u \sigma_y \sigma_z} exp - 0.5\left(\frac{y}{\sigma_y}\right)^2 * exp - 0.5\left(\frac{H}{\sigma_z}\right)^2 \quad (12)$$

For conditions of y = 0 and z = 0, which correspond to the line on the ground directly under the center of the plume, the exponential term with y drops out of Eq. (11) to give Eq. (13).

$$c = \frac{Q}{\pi u \sigma_y \sigma_z} exp - 0.5\left(\frac{H}{\sigma_z}\right)^2 \quad (13)$$

And for z = 0 and some distance y, Eq. (14) can be used. This equation is used in a feedlot dust study by Texas A&M [26].

$$c = \frac{Q}{2\pi u \sigma_y \sigma_z} exp - 0.5\left(\frac{y}{\sigma_z}\right)^2 \quad (14)$$

6.2.1 Effect of Air Dispersion Coefficients

Using the box model equation with inputs: wind=3m/s, H=4m, W=L=100m, C=200ug/m³, and Class D dispersion coefficients we get a dust flux rate of 24ug/m²/s. Using the Gaussian air dispersion equation with parameter Y ranging from -20 to +20 meters we can show the influence for each class of dispersion coefficients (Fig. 40).

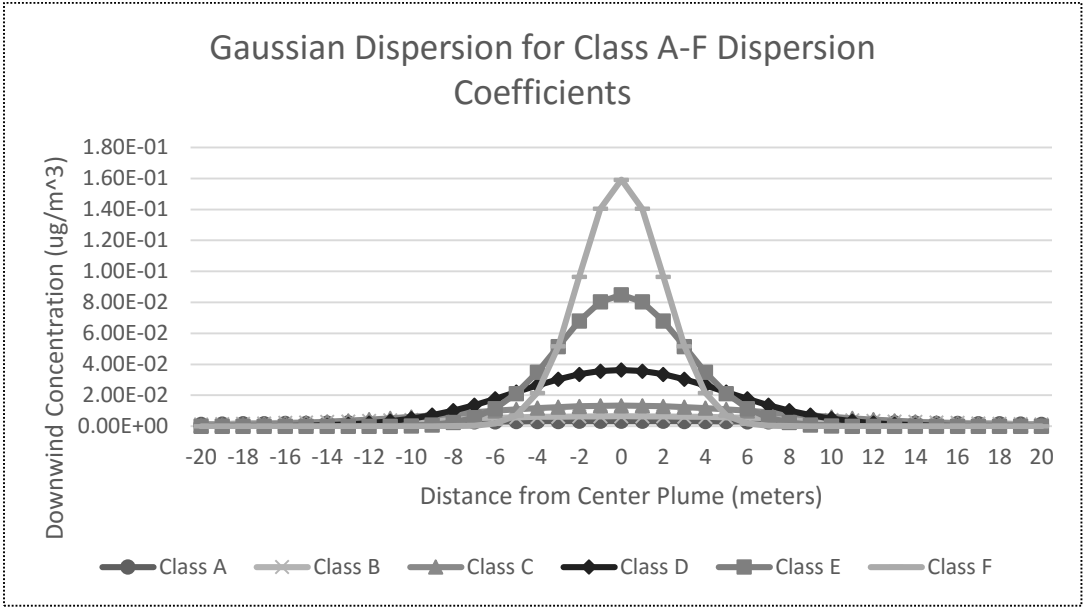

Figure 40: Effect of air dispersion coefficients

The dispersion coefficients are a function of downwind distance and class type. Table 5 shows the dispersion coefficients for each atmosphere stability class at a downwind distance of 100 meters as read from charts [25]. Class A-F is respectively: Extremely Unstable, Moderately Unstable, Slightly Unstable, Neutral, Slightly Stable, and Moderately Stable.

Table 5: Dispersion Coefficients

Air Dispersion Coefficients (meters)			
$\sigma_y$at 100m		$\sigma_z$at 100m	
CLASS A	26	CLASS A	15
CLASS B	18	CLASS B	11
CLASS C	12	CLASS C	8
CLASS D	7	CLASS D	5

CLASS E	5	CLASS E	3
CLASS F	4	CLASS F	2

6.3 Modeling Dust Plume with Box and Gaussian Models

The box model assumes a uniform distribution of dust. If an actual dust plume was uniform then a single sensor would be enough to measure the concentration. A uniform dust distribution is not common for a ground area source such as a cattle feedlot. The environmental conditions that lead to dust plumes are by their nature turbulent and not steady state. Dust generated by livestock hooves on the ground or bursts of wind would tend to be cyclic or varying over time. Concentrated aerosol will spread with wind. As a plume expands its concentration near the perimeter decreases as it combines with clean air. A normal distribution can be used to model a non-uniform dust plume.

To convert a normally distributed concentration to be used in the box model the average value of the distribution can be used. If a single sensor is used to characterize this dust plume and estimate the downwind concentration then it must be placed at a location representing the average value of the distribution. Any other placement would not accurately produce the downwind concentration.

Since a sensor such as a TEOM is large, heavy, and tethered to a power source, moving it around the plume area is nearly impossible. Therefore, there will always be some error in placing the sensor at the location of average concentration. The location with the average value should be somewhere between the lowest and highest concentration locations.

This section will model a uniformly distributed and normally distributed dust plume to show that when measuring a uniformly distributed dust plume a single accurate sensor is all that is needed, and when modeling a normally distributed dust plume or time varying plume a network of low cost and less accurate sensors will result in less error than a single accurate sensor (or reference sensor – a generally accepted sensor type accepted by the regulation organizations).

6.3.1 Uniform Distribution

In the ideal case where the actual dust plume from a ground area source is near uniform a single high precision sensor is good enough. No other sensors are necessary and additional measurement data is not helpful; it would only be redundant or serve to verify the correct operation of the single sensor.

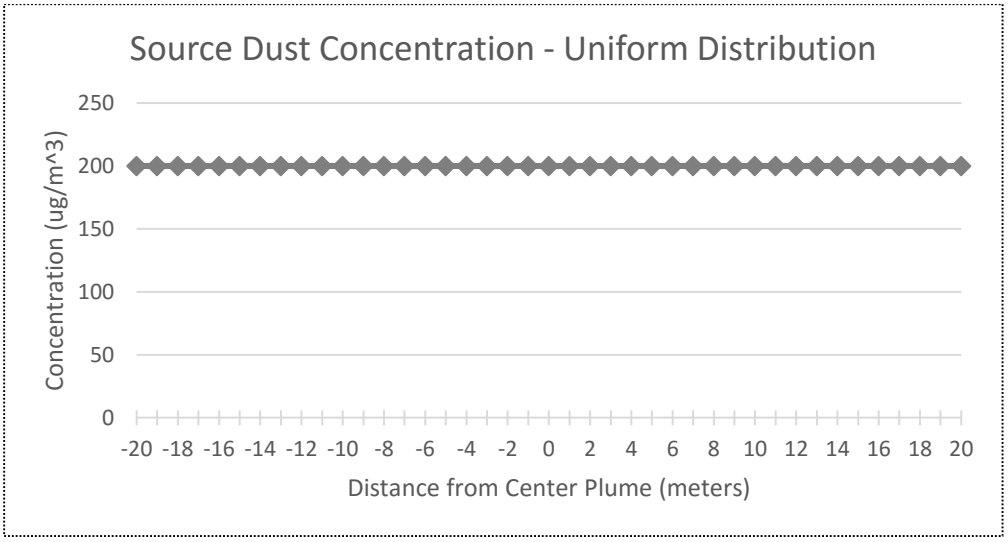

Figure 41: Uniform distribution source concentration

Figure 41 shows a uniform distribution. It does not matter where the sensor is placed in the dust plume because the plume is near uniform. Placement anywhere will yield the same measurements and result in the same downwind concentrations. Figure 42 shows an example of the downwind concentration as calculated by the Gaussian model using Class D dispersion coefficients.

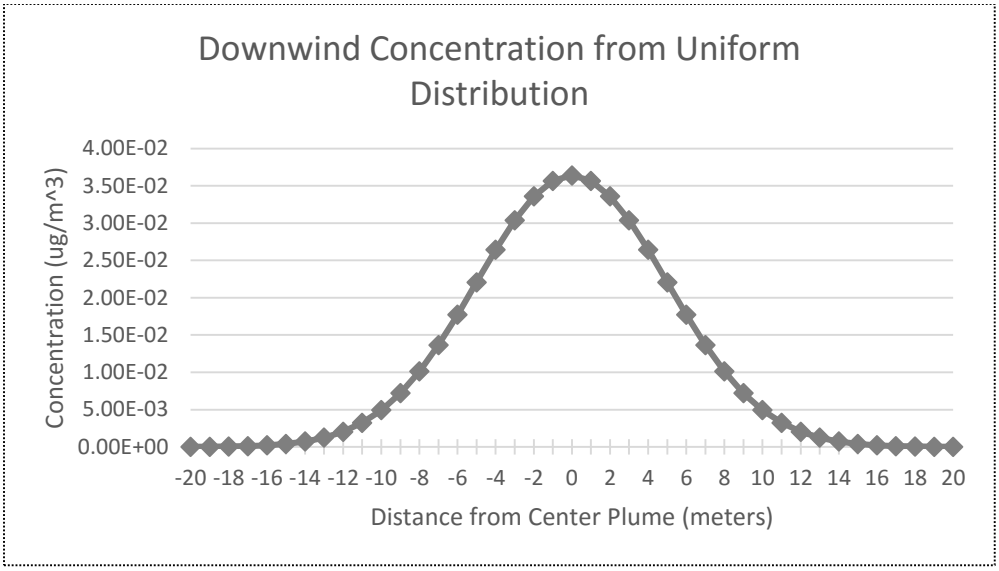

Figure 42: Gaussian downwind concentration from uniform source distribution

6.3.2 Normal Distribution with Single Sensor

A dust plume with some height and width can approximated with the curve of a normal distribution as shown in Fig. 43. An average of the normal distribution is taken to approximate a uniform distribution to be used in the box model.

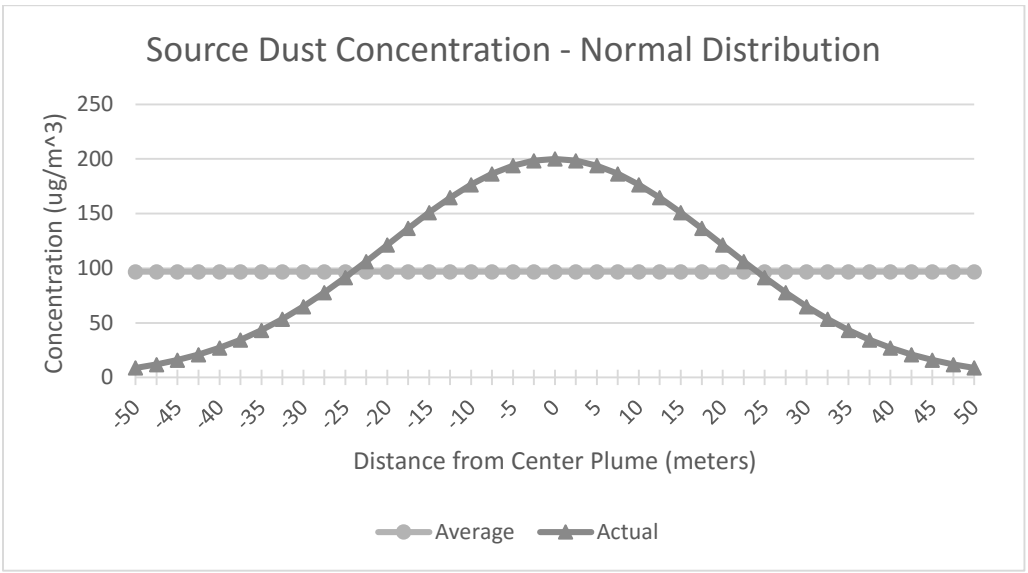

Figure 43: Normally distributed source concentration

Figure 44 shows the error in concentration as percentage for this example plume from placing a single sensor at one meter increments across the box model y-axis. The percentage error is the same for source concentration and downwind concentration when

the error is carried through the Gaussian equation. A 20% error at the source will yield a 20% error at the downwind concentration. If the sensor was placed at a particular location in a dust plume of normal distribution, then the error is that sensor value minus the average value of the normal distribution. The average concentration in this example is 96.8 ug/m³. At points 10 meters from the center plume the single sensor measurement would be close to the average plume value resulting in low error. To be within ±10% error the sensor would have to be approximately within a 1.5 meter window of the location having the dust plume average concentration. To be within ±20% accuracy it must be placed within about a 3 meter window of the point representing the average plume value. From this location, the error increases quickly as the sensor placement moves toward the center plume or toward the box edge and can have error up to about 105%.

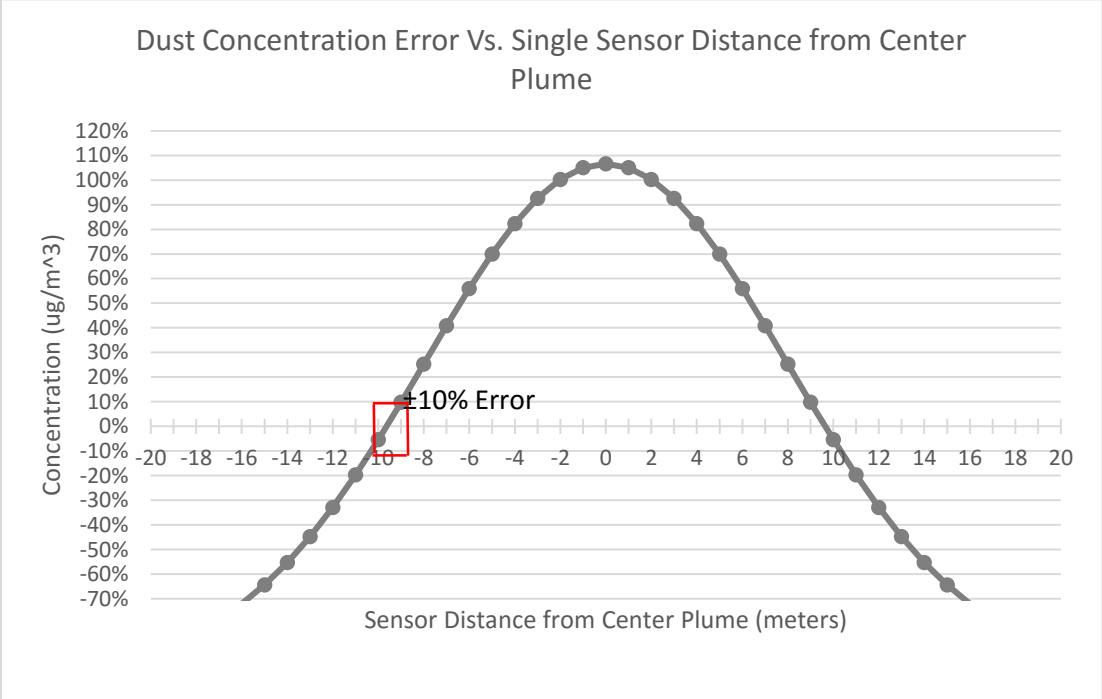

Figure 44: Single sensor error vs. sensor position

6.3.3 Normal Distribution with Sensor Network

It was shown in the previous example that to have an accuracy of less than ±20% with a single sensor it must be placed within about 3 meters of the location having the average concentration value in the normally distributed dust plume. Measuring this in the

field would be very challenging as it would be difficult to predict within 3 meters where the average concentration location will be and may also impossible to place a large reference sensor there given the environment of the cattle feedlot. If the expected location happened to be in the center of a cattle pen, it is difficult to get power there and to keep the cattle from damaging the sensor. Over time the desired location would move around as well.

Three ways a network of portable, inexpensive, and less accurate sensors can assist in obtaining more accurate data are listed. They are discussed in the next sections.

1) Place a network of sensors around the plume area in defined incremental distances so the shape of the dust plume concentration is obtained. Even if the low–cost networked sensor's accuracy is 20%, the result of finding the shape of the dust plume may lead to a more accurate value than the poor placement of one accurate sensor.
2) Place one accurate sensor in the plume along with a sensor network at defined distances around the plume. Use the accurate sensor to calibrate the data and use the multi-sensor data to find the shape of the dust plume.
3) A sensor network can measure the shape of the plume showing the time varying nature of the plume and more accurately produce the plume average concentration.

6.3.3.1 Network Sensors Only

Placing multiple low-cost sensors along the width of the box model area and simulating concentration data will show approximately how well this method can estimate the plume concentration. The sensors will sample the theoretical dust concentration curve at defined distance increments. The samples will add 20% to account for a maximum sensor error. The below diagram shows the network of sensors and a single sensor are placed in the box model. Both uniform and non-uniform plume concentrations are shown in Fig. 45.

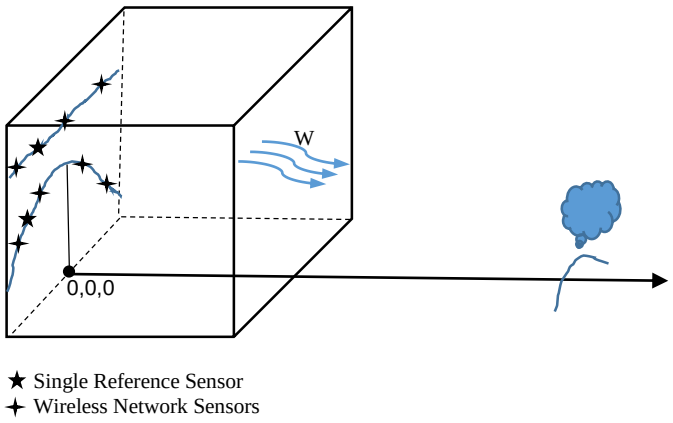

Figure 45: Box Model sensor placement

The next analysis will see how well only six sensors positioned at equal distances throughout the 100m width of the box reconstructs the original normally distributed concentration. Sensors are placed at distances -50, -30, -10, +10, +30, +50 meters from center plume. Assuming each sensor has at worst case 20% error and overestimates the actual concentration we can add 20% error to each sensor sample. These six samples are shown as diamond points in Fig. 46.

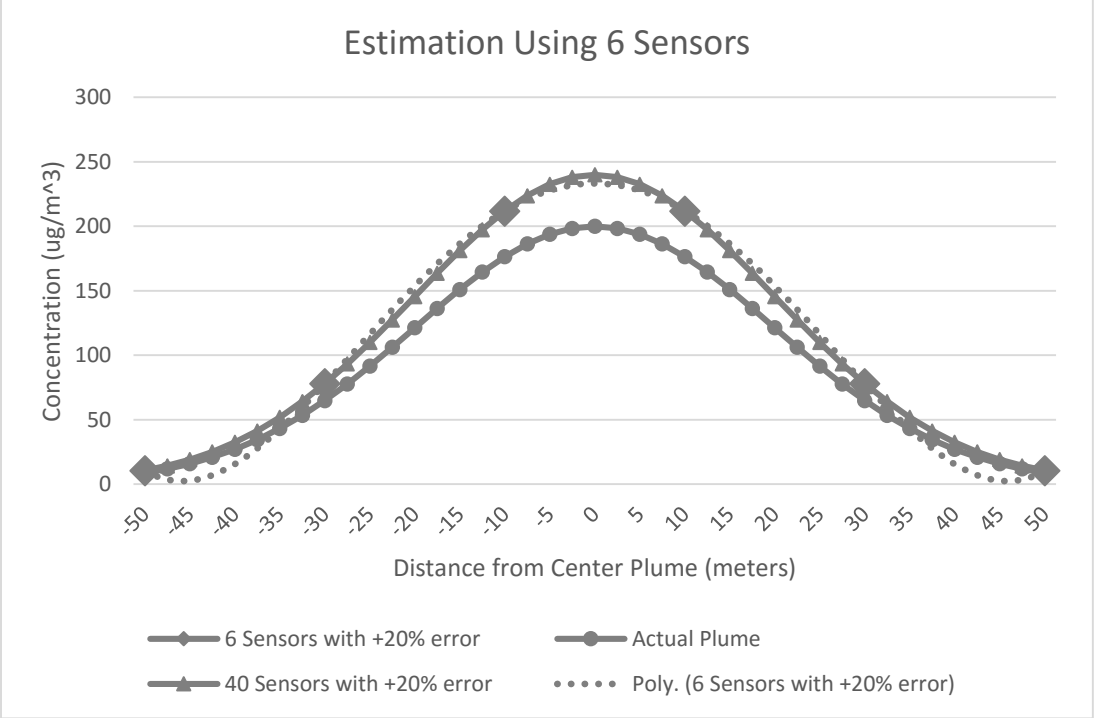

Figure 46: Estimating plume with six network sensors

The 40 sensor samples with +20% error are graphed as well. A 4th order polynomial trendline is added to the six sensor data points. The result is a line that very closely resembles the 40 sensor line. The RMSE between the two is 9.01 ug/m³. In the range of 200 ug/m³ this is only 4.5% error to the 40 sensor data.

The average value of the actual plume is 96.8 ug/m³ (Table 6). The average value of the 4th order polynomial trendline applied to the six sensors is 113.0 having an error of 16.5%. This should be worst case error, actual sensors would not all report at their maximum error for every sample. The accuracy of the six sensor average is coincidental with the shape of the plume. It underestimates the fitted trendline and since the sensor's had 20% error added it balance out to be near the actual average. This would not be accurate if the sensor's had -20% error; then it would underestimate the actual average and result in much larger error.

Table 6: Network Sensors Plume Accuracy

Signal	Average (ug/m³)	Average Error (ug/m³)	Average Error	RMSE
Actual	96.8	0	0%	
6 Sensors	100.0	3.2	3.3%	
40 Sensors	116.2	19.4	20.0%	9.01
6 Sensor Poly Trendline	113.0	16.2	16.5%	

6.3.3.2 Network Sensors and Single Reference Sensor

This method will use the single reference sensor to calibrate the trendline through the data samples collected by the low-cost sensor network. Placing the reference sensor at the same location as one of the network sensors should result in better scaling of the trendline since the trendline holds tighter to these points. Figure 47 shows the result of scaling the sensor trendline to the reference sensor using the data from the previous example. In this case the scale factor is 20%.

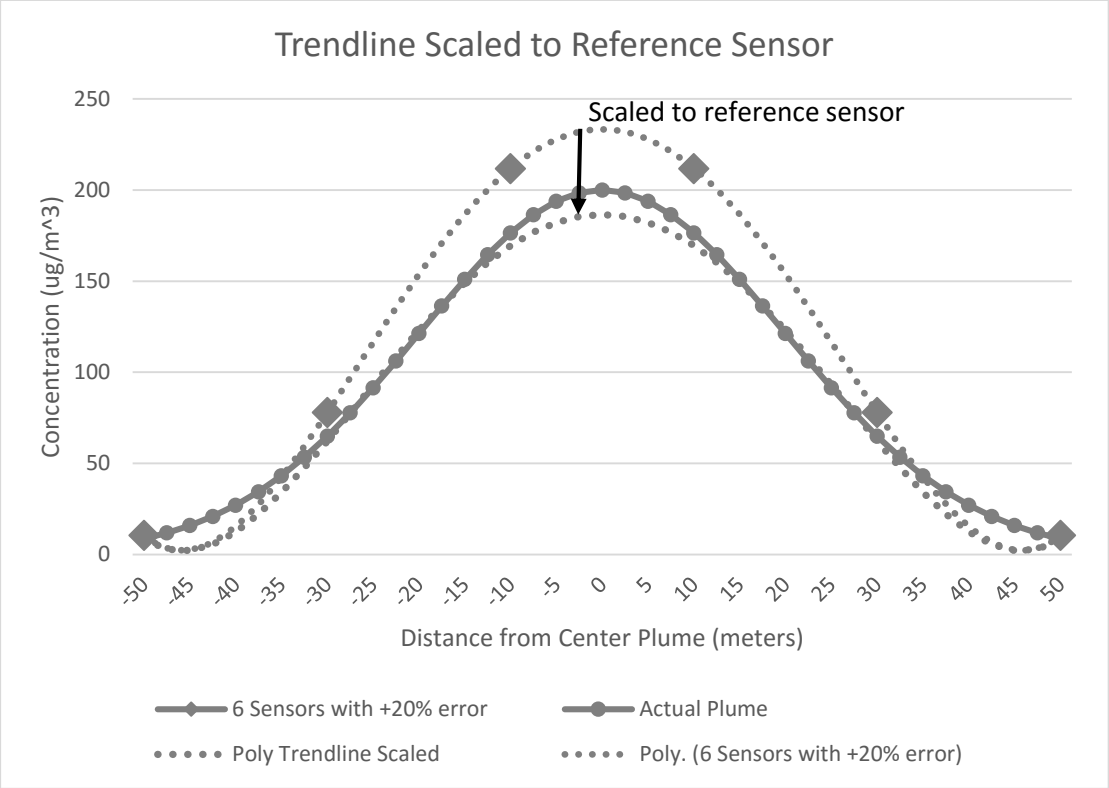

Figure 47: Scaling six sensor trendline for reference sensor

For the box model it is important that the average value of the scaled data accurately represents the average of the dust plume. In this example, after scaling the trendline of six sensors to the reference sensor the error of the average is 6.6%. The root mean square error (RMSE) is 8.74 compared to 24.9 before scaling. This method results in the lowest average error and the lowest RMSE value. The standard deviation of the error is 5.93. These values are summarized in Table 7.

Table 7: Network Sensors and Reference Sensor Plume Accuracy

Signal	Average (ug/m^3)	Average Error Percent	Standard Deviation of Error	RMSE to Actual
Actual	96.8	0%	0	0
6 Sensors	100.0	3.3%	18.9	21.7
40 Sensors	116.2	20.0%	13.4	23.5

6 Sensor Poly Trendline	113.0	16.5%	8.43	24.9
Scaled to Reference	90.4	6.6%	5.93	8.74

6.3.3.3 Network Sensors with Time-Varying Plume

Many field studies using the box model ignore the time-varying nature of dust plume concentration since one of its base assumptions is that the concentration be constant in the box. Another approach to this is to treat the constant box concentration as several discrete samples and average them together. This is also done for changing weather factors during a study. Figure 48 shows the box model with time-varying concentration.

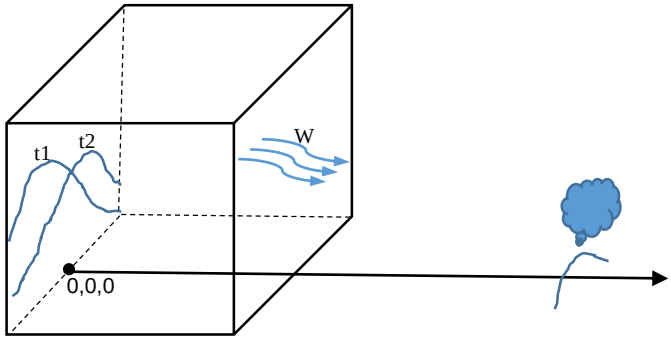

Figure 48: Box Model with time-varying plume

A time-varying plume is considered next. To model this, both the center position and max concentration of the plumes are changed linearly with time. Figure 49 shows five discrete plumes for times T1-T5. From T1 to T5 the amplitude decreases by 16% and the center plume shifts position by 16%. The box-shaped points represent the six network sensors at fixed locations distributed evenly throughout the 100 meter field width. The diamond shaped points represent the single reference sensor at a fixed location. The dotted lines are 4^{th} order polynomial trendlines fitted to the six networked sensors.

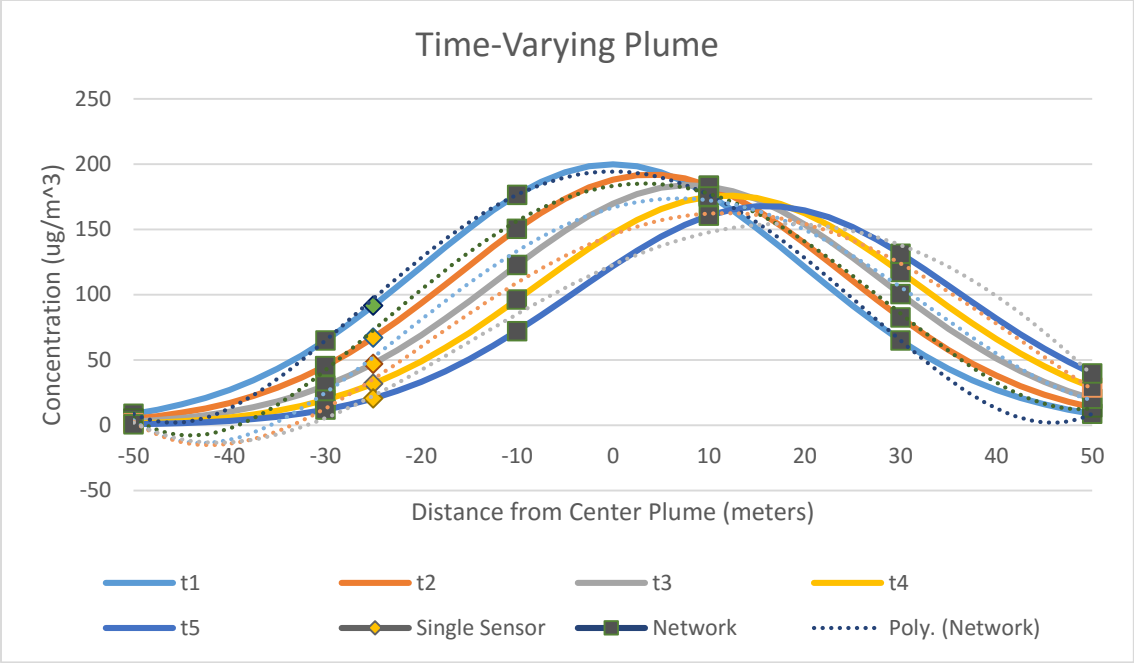

Figure 49: Modeling time-varying plume

The average of all the trendlines of the six networked sensors with no additional sensor error added has error in concentration measurement at 3.2% from the average of actual plume lines. This shows the basic approach of averaging trendlines is accurate. Taking the six sensors all at worst case error of 20%, and applying this method of averaging the trendlines resulted in 22.3% error. The single reference sensor had the highest error at 41%. So the method using six sensors with 20% error added is only 54% of that of the error from using a single reference sensor. Table 8 summarizes these error values.

Table 8: Network Sensors Time-Varying Plume Accuracy

Timestamp	Actual Average	Single Sensor Sample	6 Sensor Points Average	6 Sensor Trendlines Average	6 Sensor +20% Error Trendlines Average
T1	96.8	91.6	83.4	89.4	112.8
T2	92.8	67.1	80.0	91.2	114.4
T3	88.5	47.2	76.6	84.6	109.2
T4	83.4	31.8	73.1	81.4	107.8
T5 Average T1-T5	78.9 88.1	20.5 51.6	69.4 76.5	79.1 85.2	94.7 107.8
Error %	0%	41%	13%	3.2%	22.3%

Chapter 7: Conclusion

Using an off-the-shelf optical sensor is an inexpensive way to build entry-level sensors for monitoring dust concentration. Calibration in a dust generation chamber is the first step toward getting accurate sensor data. The construction and operation of a dust generation chamber was detailed and a calibration method of using the falling edge of the dust peak was proposed.

Ten nephelometers were constructed for a field test performed at a cattle feedlot site in Texas. A twelve-hour test was run during a typical peak-dust period. It was discovered from field testing that there is an issue with dust collecting on the sensor optics and sensing region. The sensor could still accurately sense spikes and fluctuation in dust concentration, but would no longer settle to a low value when the air dust concentration receded.

The average sensor error in the first five hours of the field test was 0.77 mg/m^3 (7%). The average error after the evening dust peak was 3.23 mg/m^3 (32%). This was a successful proof of concept showing that an inexpensive sensor combined with a simple circuit, wireless communication capability, battery power, and at 2% of the cost of a TEOM sensor can provide enough resolution in measurement to be useful for field studies, particularly, to provide more points of measure at a lower cost. Further refinements in construction and calibration on this sensor could easily improve its accuracy over the test duration.

A microscope sensor was designed to capture dust concentration information in a new way while maintaining a low cost position. The sensor used the method of impaction to collect dust samples and piped them through the imaging region of a high magnification USB microscope. When the pumping of the dust filled liquid stopped, images were captured and collected for processing.

An image processing algorithm was developed to convert image data into dust particle mass. To process an image, the average background was subtracted, then a threshold was applied followed by a median filter. Connected Component Labeling was implemented to separate particles into individual regions. The region's size was measured using the Equal Area Projection method to get a particle diameter. A mass equation used

particle density and diameter to calculate the particle's mass. Lastly, all the particle masses on an image were summed together and logged in a .csv file.

The trending data on the accumulated mass graph with less than 33% error shows that this sensor design has promise. A problem was very few particles were captured in images with this design. With improvements sampling efficiency to increase the particle count in the images, it should be possible to get a reasonably accurate real-time output of particle mass and concentration. A unique aspect of using an image sensor is that additional information can be easily obtained such as particle size, shape, color.

By modeling dust plumes as uniform and normal distributions it was shown that there is a benefit of using a network of low-cost, lower accuracy sensors. A single sensor is very dependent on its placement in a plume and therefore is less accurate in non-uniform plumes and time-varying plumes. The modeling shows that a network of six sensors placed evenly across the field width all reporting a max error of 20% can still obtain a plume average concentration with 16% max error. If one reference sensor is added near one of the network sensors for scaling purposes then the sensor network error is brought down to 6.6%. Six network sensors measuring a time-varying plume produced an error in average concentration of 22% compared to 41% error from a single reference sensor.

Overall, combining low-cost wireless network of sensors with existing reference sensors can produce a more detailed model of a dust plume and result in a more accurate average concentration for non-uniform plumes. Obtaining dust particle shape and size information from a microscopic sensor could help in understanding the plume model behavior related to environmental weather condition.

7.1 Future Recommendations

The nephelometer sensor could be improved by designing a method to clean the dust accumulation on the sensor internals. Perhaps a burst of compressed air would be sufficient to remove the buildup. A different method to combat dust accumulation could be to apply a zero filter to the input of the sensor and recalibrate it on the fly. A zero filter would not allow any particles through and the sensor could calculate a new offset value.

Wind direction across the inlet of the sensor also affects its accuracy. Developing a specialized inlet that doesn't depend on wind direction would be useful. Perhaps a wind vane could be used to keep the sensor inlets on all the sensors pointing in the same direction.

The microscope sensor could be improved by increasing the sampling efficiency of the dust collection method. Other methods could be attempted such as combining the air stream with a pressurized mist, or even bubbling the air up through a water reservoir. The dust sampled should be an accurate representation of the dust concentration in the air.

Another improvement for this sensor would be to increase the speed at which images are collected. The maximum capture rate of this USB microscope was 30Hz. With more financial investment, an industrial image sensor that is capable of very high speed could be used. With high speed image capture the micropumps would not have to stop pumping to capture a still image. Every particle captured at the sampling area could be imaged and processed maximizing the sensor accuracy.

A field study should be performed to verify the wireless sensor network's ability to enhance the plume information from a single reference sensor. Actual plume measurement of concentrations are various heights and widths can be used as an input source to the modeling examples.

References

[1] Cattle Empire. *In the Heart of the Beef Feeding Empire.* Accessed August 8, 2015, from: http://www.cattle-empire.net/.

[2] United States Environmental Protection Agency. (2014, October 21). *National Ambient Air Quality Standards (NAAQS).* Accessed August 8, 2015, from: http://www.epa.gov/air/criteria.html.

[3] SKC, Inc. *Inhalable Particulate Mass.* Accessed August 8, 2015, from: http://www.skcinc.com/catalog/infopage.php?id=9020.

[4] Extension. *Health Impacts of Air Emissions from Animal Feeding Operations*. Accessed August 8, 2015, from: http://www.extension.org/pages/67058/health-impacts-of-air-emissions-from-animal-feeding-operations.

[5] Extension. (2015, February 3). *Air Quality Resources for Policy Makers*. Accessed August 8, 2015, from: http://www.extension.org/pages/66999/air-quality-resources-for-policy-makers.

[6] Wanjura, J.D., Parnell, C.B. Jr., Shaw, B.W., Lacey, R.E., Capareda, S.C., & Hamm, L.B. (2005). *Comparison of Continuous Monitor (TEOM) vs. Gravimetric Sampler Particulate Matter Concentrate.* ASAE Paper No. 054048. Accessed August 8, 2015, from http://cafoaq.tamu.edu/files/2012/01/PU01105_6.pdf.

[7] Jiayin, Li, Qijia, Ying (2007) On-Line Monitoring Device of Airborne Particulate Concentration Based on The Principle of Vibration. *8th International Conference on Electronic Measurement and Instruments*.

[8] United States Department of Labor. *Air Sampling and Analytical Procedures for Determining Concentrations of Cotton Dust.* Accessed August 8, 2015, from: https://www.osha.gov/pls/oshaweb/owadisp.show_document?p_table=STANDARDS&p_id=10054.

[9] Malvern. *Laser Diffraction: Particle Size Distributions from Nanometers to Millimeters.* Accessed August 8, 2015, from: http://www.malvern.com/en/products/technology/laser-diffraction/.

[10] TSI Incorporated. (2012). *Dusttrak II Aerosol Monitor Theory of Operation*. Accessed August 8, 2015, from: http://www.tsi.com/uploadedFiles/_Site_Root/Products/Literature/Application_Notes/EXPMN-001_DustTrakII_Theory_of_Operation.pdf.

[11] Fu, Y., & Hallberg, B. (2010). A Personal Environment Monitoring System Pulmonary Disease. *Bioinformatics and Biomedical Engineering (ICBBE), 2010 4th International Conference*, 1-4.

[12] Fu, Y., Ayyagari, D., & Colquitt, N. (2009). Pulmonary Disease Management System with Distributed Wearable Sensors. *Engineering in Medicine and Biology Society, 2009. EMBC 2009. Annual International Conference of the IEEE*, 773-776.

[13] Chowdhury, Z., Edwards, R.D., Johnson, M., Shields, K.N., Allen, T., Canuz, E., & Smith., K.R. (2007, July 20). An Inexpensive Light-Scattering Particle Monitor: Field Validation. *Journal of Environmental Monitoring*, *9*, 1099-1106.

[14] Jiaying, L., Qijia, Y. (2007). On-Line Monitoring Device of Airborne Particulate Concentration Based on the Principle of Vibration. *Electronic Measurement and Instruments, 2007. ICEMI '07. 8th International Conference*, 261-264.

[15] Budde, M., Berning, M., Busse, M., Miyaki, T., & Beigl, M. (2012). The TECO Enviboard: A Mobile Sensor Platform for Accurate Urban Sensing and More. *IEEE 2012*.

[16] Weekly, K., Rim, D., Zhang, L., Bayan, A.M., Nazaroff, W.W., & Spanos, C.J. (2013). Low-Cost Coarse Airborne Particulate Matter Sensing for Indoor Occupancy Detection. *IEEE International Conference on Automation Science and Engineering 2013*, 32-37.

[17] Li, L., Zheng, Y., & Zhang, L. (2014). Demonstration Abstract: PiMi Air Box: A Cost-Effective Sensor for Participatory Indoor Quality Monitoring. *IPSN '14 Proceedings of the 13th International Symposium on Information Processing in Sensor Networks,* 327-328.

[18] Kim, S. & Paulos, E. (2009). InAir: Measuring and Visualizing Indoor Air Quality. *ACM 2009.*

[19] Soldo, D., Quarto, A., & Di Lecce, V. (2012). M-DUST an Innovative Low-Cost Smart PM Sensor. *Instrumentation and Measurement Technology Conference (I2MTC), 2012 IEEE International,* 1823-1828.

[20] Holstius, D.M., Pillarisetti, A., Smith, K.R., & Seto, E. (2014, April 30). Field Calibrations of a Low-Cost Aerosol Sensor at a Regulatory Monitoring Site in California. *Atmospheric Measurement Techniques, 7,* 1121-1131.

[21] Gill, T.E., Zobeck, T.M., and Stout, J.E., (2006). Technologies for laboratory generation of dust from geological materials. *Journal of Hazardous Materials* 132: 1- 13.

[22] Meinhart, C.D., Wereley, S.T., & Santiago, J.G. (1999). PIV Measurements of a Microchannel Flow. *Experiments in Fluids, 27,* 414-419.

[23] Wikipedia. *Connected Component Labeling.* Accessed August 8, 2015, from: https://en.wikipedia.org/wiki/Connected-component_labeling

[24] Learning Objective Module, E-Learning Courses from the IITs & IISC. Accessed November 30, 2015, from: http://nptel.ac.in/courses/Webcourse-contents/IIT-Delhi/Environmental%20Air%20Pollution/air%20pollution%20(Civil)/Module-5/1.htm

[25] Air Pollution Concentration Models. Accessed November 30, 2015, from: http://shodor.org/media/content/hpcu/website/resources/xsede14/AirPollutantConcentrationModels

[26] Goodrich, L. B., C. B. Parnell, R. E. Lacey, S. Mukhtar, and B. W. Shaw. 2003. Evaluation of the use of the box model to determine emission fluxes from area sources and the corresponding modeled concentrations using the industrial source complex. *In Proc. 2003 Beltwide Cotton Conference.*

[27] Madhoun, W. A., Air Quality Modeling. Accessed November 30, 2015, from: http://site.iugaza.edu.ps/wmadhoun/files/1-Air-Quality-Modeling2.ppt

Appendix A Nephelometer Hardware Specification and BOM

Nephelometer Specification

Sensor Type	Angled Light Scattering
Range	Calibrated to 0.00 to 16.00 mg/m³
Resolution	±0.02 mg/m³
Particle Size Range	Approximately 0.1 to 10 µm
Flow Rate	0.424 CF
Operational Temp	Above 32 °F (0 °C)
Operational Humidity	Non-condensing
Log Interval	Adjustable 1, 2, 5, 10 seconds
Data Logging	*79 days,10 sensors ,logging interval 1 sec
Physical Size	5.3 x 6.3 x 2.0 in. without battery 5.3 x 6.3 x 4.0 in. with battery
Weight	Sensor < 1 lb Battery 12 oz.
Communications	RS-232, 9600 baud, driven, inverted 802.15.4, 2.4 GHz
Wireless Range	Up to 1 mile, Outdoor Line of Sight
Power	10-20 VDC
Battery	11.1 V Li-Ion 4400mAh Life, 3-4 days, 1 second logging interval, PL=3

* to estimate how many days the data logger can collect data use equation: 792* Ts / N = # days; where Ts = 1,2,5,10

Nephelometer BOM

Description	Manufacturer	Manufacturer P/N	Qty	Price Each	Total
PCB BOM					
PIC2455	Microchip Technologies	PIC18F2455-I/SO	1	6.04	6.04
diode	Fairchild Semiconductor	S1G	1	0.53	0.53
20MHz crystal	Abracon Corporation	ABM3-20.000MHZ-B2-T	1	1.88	1.88
5V regulator	STMicroelectronics	L78L05ABUTR	1	0.81	0.81
8V regulator	NJR	NJM78L08UA#	1	0.47	0.47
3.3V regulator	Sharp Mincroelectronics	PQ1L333M2SPQ	1	0.81	0.81
2mm header (Xbee)	Sullins Connector Solutions	NPPN101BFCN-RC	2	1.05	2.1
LED	Panasonic SSG	LN276RPX	1	0.27	0.27
Voltage Converter	Texas Instruments	SN74LVC04ADR	1	0.47	0.47
conn board to sharp	Sullins Connector Solutions	PPPC061LFBN-RC	1	0.56	0.56
Xbee Pro, wire ant	Digi International	XBP24-AWI-001	1	32	32
Raw PCB, Purch Qty 100	Sunstone Circuits		1	7	7
Resistors					
75, 1206	Generic	5%, 50V, 1206	1	0.08	0.08
300, 1206	Generic	5%, 50V, 1206	1	0.08	0.08
1k, 1206	Generic	5%, 50V, 1206	3	0.08	0.24
3.4k, 1206	Generic	5%, 50V, 1206	1	0.08	0.08
10k, 1206	Generic	5%, 50V, 1206	1	0.08	0.08
20k, 1206	Generic	5%, 50V, 1206	1	0.08	0.08
22k, 1206	Generic	5%, 50V, 1206	1	0.08	0.08
62k, 1206	Generic	5%, 50V, 1206	1	0.08	0.08
Capacitors					
18 pf, 1206	Kemet	C1206C180J5GACTU	2	0.23	0.46
0.01 uf, 1206	Generic	20%, 50V, 1206	1		0.24
0.1 uf, 1206	Generic	20%, 50V, 1206	6		1.44
0.33 uf, 1206	Generic	20%, 50V, 1206	2		0.48
1.0 uf, 1206	Generic	20%, 50V, 1206	1	0.24	0.24
10uf, 1206	Generic	20%, 50V, 1206	1		0.24
100uf, radial thru hole	Generic	20%, 50V, 1206	1		0.24
				Subtotal	**57.08**

Sensor Box Build					
Sharp sensor	Sharp	GP2Y1010AU0F	1	11.38	11.38
small fan	Copal Electronics Inc	F16EA-03LLC /E	1	11.16	11.16
small box	Hammond Manufacturing	1594ASGY	1	4.54	4.54
large box	Bud Industries	CU-1874-G	1	3	3
Power connector	CUI Inc	PJ-011A	1	1.89	1.89
Sharp Connector	JST Sales America Inc	ZHR-6	1	0.1	0.1
Sharp Connector	JST Sales America Inc	SZH-003T-P0.5	6	0.02	0.12
R/A conn 36 pins	Sullins Connector Solutions	PEC36SBAN	0.16	1.71	0.29
wire to sensor 100'	Alpha Wire Company	1852 WH005	0.03	36.9	1.11
DB9 connector	Norcomp Inc	1734348-1	1	0.95	0.95
PVC port cover 6'	Menards		0.083	3	0.25
Dust Cap DB9	Norcomp Inc	160-000-209R000	1	1.08	1.08
				Subtotal	**92.95**
Battery Box Build					
Battery	batterySpace.com		1	59.95	59.95
Charger	batterySpace.com		1	24.95	24.95
Battery Box	Bud Industries	CU-1874-G	1	3	3
Battery DC Plug	CUI Inc	PP3-002AH	1	1.82	1.82
DC for charger	CUI Inc	PJ-011A	1	1.89	1.89
				Subtotal	**91.73**
				Grand total=	**184.56**

Appendix B Microscope Sensor BOM

Item	Description	Vendor	P/N	Qty	Price Each	Total
1	Scope Stand	PCGears.com	MS34B	1	$ 69.00	$ 69.00
2	Dino-Lite Scope 500X	PCGears.com	BIGC-AM413MT5	1	$ 669.00	$ 669.00
3	Micropump	Micro-Components.com	MP6	2	$ 25.00	$ 50.00
4	pump eval board	Micro-Components.com	MP6-EVA	2	$ 50.00	$ 100.00
5	tubing 3m	Micro-Components.com	MPT	1	$ 10.00	$ 10.00
6	check valve	Micro-Components.com	MP-CV	1	$ 10.00	$ 10.00
7	0.03mm capillary tube 33/vial	FDGlass.com	BMS-003-03-025-100	0.03	$ 46.00	$ 1.38
8	6mm capillary tube	FisherSci.com	S37615B	1	$ 14.00	$ 14.00
9	plastic bottle	Mcmaster.com	42305T33	2	$ 1.55	$ 3.10
10	needle assortment	Mcmaster.com	75165A791	1	$ 27.00	$ 27.00
11	tubing 6mm ID, 9mm OD, 1ft	Mcmaster.com	5054K14	2	$ 0.92	$ 1.84
12	barbed coupler female 10/pack	Mcmaster.com	51525K141	1	$ 4.28	$ 4.28
13	threaded coupler	Mcmaster.com	51525K234	1	$ 5.91	$ 5.91
					Subtotal	$ 965.51

Appendix C DGS Bill of Materials

Item	Qty	Ref	Description	Cost Each	Ext. Cost
1	2	A	3/4" PVC Ball Valve	$1.99	$3.98
2	2 ft	B	3/4"x6' PVC Pipe	$6.99	$2.33*
3	2	C	1"x3/4" PVC Bushing	$0.52	$1.04
4	2	D	1" PVC Adapter w/nut	$1.49	$2.98
6	1	E	4'x8' x1/4" Acrylic Sheet	$89.97	$89.97
7	1	F	1/4" Tubing Valve	$6.98	$6.98
8	3 ft	G	.17" ID x 10' Vinyl Tubing	$1.40	$0.42*
9	1	H	Osterizer Blender	$24.00	$24.00
10	1	I	Dust Shield Baffle		**
11	1	J	Vacuum Nozzle Kit	$12.88	$12.88
12	1	K	Shop Vacuum	$47.98	$47.98
13	80 in	L	Aluminum Angle 1/16"x3/4"x3'	$3.67	$8.16
14	12	M	7/8" Closed S-Hook	$1.59	$3.18
15	12	N	4-5/32x3/4" Spring	$1.59	$19.08
16	24	O	8-32x3/4" bolts, 75pc	$2.97	$2.97
17	80 in	P	17' Gasket Grey	$3.57	$1.40*
18	1	Q	1/4" Acrylic Lid		**
19	1		4 oz. PVC Cement	$2.78	$2.78
20	1		Vacuum Filter Cartridge	$9.88	$9.88
21	1		Acrylic Bonding Agent	$5.00	$5.00
			Total		$245.01

*Price for partial material

**Price included from another item